Russian Chemical Reviews **72** (10) 823 – 847 (2003) © 2003 Russian Academy of Sciences and Turpion Ltd

DOI 10.1070/RC2003v072n10ABEH000805

Fractal structures in disperse systems

V I Roldughin

Contents

I.	Introduction	823
II.	Fractal aggregates	824
III.	Kinetics of coagulation of fractal aggregates	829
IV.	Multifractal analysis of fractal aggregates	832
V.	Fractal gels and emulsions	836
VI.	Two-dimensional fractal structures	838
VII.	Viscous fingering	840
VIII.	Fractal films	841

Abstract. The fractal structures that form in disperse systems are considered. Theoretical models of fractal aggregation and the kinetics of coagulation of fractal aggregates are described. The characteristics of deposited fractal films and of corroded surfaces are considered. The multifractal analysis of colloidal systems and related thermodynamics of fractal aggregates are outlined. The bibliography includes 380 references.

I. Introduction

The concepts of fractal structures or, simply, fractals have been widely used since the 1980s. Fractals are objects that are characterised by a fractional dimension. Pioneering studies on mathematical treatment of objects with fractional geometric dimensions date back to the early 20th century; however, they have rarely been the subject of physicochemical research. It was Mandelbrot who clearly demonstrated in his monographs [1, 2] that many systems in nature can be considered as fractals. This aroused the interest of physicists and chemists in fractal structures.

The most important property of fractal structures is self-similarity. The visual appearance of self-similar structures is identical at different length scales, which allows one to envision the structure of the whole object using a fragment of it. Since this property is also characteristic of many non-fractal structures, the second property of fractals becomes of crucial importance. Namely, the changes in various characteristics (mass, density, surface area, elastic modulus, *etc*.) of a fractal object, which are due to changes in the size of the object or in the corresponding length scale, obey a power law with a fractional exponent. In other words, some relationships established for conventional one-, two- or three-dimensional systems are valid for fractals if we assume that their geometric dimension is not an integer.

The concepts of fractals have provided a better insight into both the structural organisation and the laws governing various nonequilibrium processes in various physicochemical systems. Simultaneously, many regularities of the changes in the physicochemical parameters with varying spatio-temporal characteristics have been revised.

The new concept of structural organisation of well-known objects gave an impetus to original experimental studies and to the development of novel theoretical models. Considerable efforts have been made in order to find, generate and examine fractal structures. It should be noted that the subjects of a large number of these studies were typical objects of colloid chemistry, namely, particle aggregates, porous media, composite materials and rough surfaces. Therefore, it is quite reasonable that the first reviews and monographs in the field concerned mainly fractal aggregates.

In spite of extensive literature on fractal objects,[3–23] many issues dealing with the properties of colloidal fractal structures are still to be clarified. Besides, a considerable body of information on the fractal characteristics of various colloidal systems has been accumulated in the last decade. Because of this, it seems appropriate to generalise the results obtained.

In this review, the emphasis is placed on the studies reported in the 1990s and more recently and on a few publications from the 1980s which contain basic results. These are necessary to enhance the integrity of material presented below.

The contents of the review is self-explanatory, so we will not dwell on its structure. Mention can only be made that here we have restricted ourselves to the consideration of (mainly) theoretical models for growth and geometric characteristics of fractal aggregates. Many problems concerning the description of experimental studies on the physicochemical properties of fractal aggregates and their dispersions will be the subject of a separate review, which will be published in the near future.

It seems appropriate to begin with a definition of the fractal dimension, which will be implicitly used throughout the text. The point is that this notion can be introduced in several ways, some of which are mathematically inequivalent. Subtle details of the corresponding mathematical treatment can be found in, *e.g*., monograph.[13] From this point on we will consider that the fractal dimension of any physical object can be determined using the following relationship †

V I Roldughin Institute of Physical Chemistry, Russian Academy of Sciences, Leninsky prosp. 31, 119991 Moscow, Russian Federation. Fax (7-095) 952 53 08. Tel. (7-095) 955 46 47.
E-mail: roldugin@phyche.ac.ru

Received 25 February 2003
Uspekhi Khimii **72** (10) 931 – 959 (2003); translated by A M Raevsky

† Here and in some relationships listed below unity is implied to be a dimensional quantity whose dimension is inverse to that of the expression under the logarithm.

$$d_f = \lim_{\delta \to 0} \frac{\ln N(\delta)}{\ln(1/\delta)},$$

where N is the number of boxes (spheres) of size δ needed to completely cover a given object (the so-called box-counting technique). Therefore, calculations of d_f in a particular case require the number of boxes of a given size necessary to cover the object to be counted and the limit of the ratio of logarithms with $\delta \to 0$ to be evaluated. In the case of planar fractal objects one can use squares (disks) instead of boxes. This relationship, adapted to particular systems, is most often used in determining the fractal dimension of physicochemical objects. Some modification of this relation will be given below. It should be noted in advance that here we will not discuss the problems concerning possible differences between the fractal dimensions determined using different relationships because they are of little interest for physical chemists. Besides, the development of fractal theory is accompanied by the introduction of various fractal dimensions, which characterise particular physicochemical properties of objects under study. Some of them will be introduced in the next Sections of the review.

II. Fractal aggregates

Aggregates of colloidal particles were among the first objects described using fractal geometry concepts. The pioneering studies on fractal clusters have been well documented in a number of reviews.[7,8,12] In this Section we will consider the main stages of development of the fractal concepts.

Interest in fractal aggregates was aroused after publication of two basic studies[24,25] concerning aggregates of highly dispersed iron particles produced by flash evaporation of induction heated wires. Analysis showed[24] that the aggregates can be treated as fractal structures, while numerical experiments using a model of diffusion-limited aggregation of individual particles revealed[25] that the process involves formation of aggregates, which possess some properties of fractals. Next, it was found that fractal aggregates can be generated in numerical experiments with various growth models[26,27] for diverse colloidal systems.[28–37] These investigations were followed by dramatic increase in the studies on the formation and structure of aggregates of colloidal particles and other fractal objects. To date, fractal aggregates of gold,[29,34] hematite,[38,39] silica,[40] polystyrene[41] and carbon[42] particles have been obtained. The state-of-the-art in the field of research on fractal structures since 1985 is well illustrated by the book,[43] which gives a clear idea of both the expansion of avenues of investigation and diversity of the methods for studying fractals.

Computer simulation has played a significant role in the studies of fractal aggregates. Detailed analysis of the available literature in the field is presented in a monograph.[18] Computer models allow different regimes of particle aggregation to be examined. They also serve as the basis for carrying out real experiments and processing large arrays of experimental data. Now it is appropriate to briefly outline the main models for description of particle aggregation, which are used in numerical simulation. We will often refer to them in the text below.

1. Classical models for fractal aggregation

Numerical experiments began with the simulation of random walk of particles on a lattice. This imposed some limitations. The next step was to simulate the motion in free space instead of the movement of particles over lattice sites. This caused no significant changes in the structure of clusters at longer length scales but led to a more realistic structural organisation of aggregates at short length scales. If numerical simulation concerns the random walk of clusters and particles on a lattice, the corresponding models are called lattice models. Otherwise (motion in continuous space), they are called off-lattice models.

The simplest model of aggregation was proposed by Eden. According to this model, a seed is initially introduced into the system, which gives rise to a cluster. Growth occurs by attachment of a particle to a randomly chosen, unoccupied nearest-neighbour perimeter site. This repeats during each step of growth simulation. The model generates a dense cluster and is therefore usually considered as a model for growth of dense objects (*e.g.*, crystals).

The ballistic model considers the motion of a pair of clusters (or a cluster and a particle) along randomly chosen linear trajectories. Collisions between clusters causes their aggregation. In the simplest version of the model the structure of the aggregate is determined by the mutual orientation of moving clusters at the instant at which they first contact each other. If the growth of a cluster occurs by attachment of single particles, the model is called the particle–cluster ballistic aggregation model. If the process of aggregation involves not only the primary particles (monomers) but also aggregates, the model is called the cluster–cluster ballistic aggregation model. The Witten–Sander model for diffusion-limited aggregation (DLA) assumes that aggregation occurs by attachment of a particle (or aggregate) to the seed (aggregate). Here, the particle (or aggregate) is introduced into the system at a rather long distance from the seed and experiences Brownian motion before collision with the seed. As particles or aggregates first contact each other, they combine irreversibly. Similarly to the ballistic model, two types of aggregation are considered, namely, particle–cluster and cluster–cluster aggregation in accord with the type of the object introduced into the system (single particle or a cluster).

Among the variety of models proposed to describe the processes of particle aggregation, the reaction-limited cluster–cluster aggregation (RLA) model is most widely used. According to this model, particles and clusters moving *via* Brownian motion must experience numerous collisions before aggregation. In numerical simulation, this is included by setting a low probability, p, of the collisional aggregation of particles. If this probability is rather high or even set to unity, the diffusion transport of particles can appear to be the limiting step and the DLA regime operates. In the limiting case ($p \to 0$), the reaction-limited particle–cluster aggregation model is transformed into the Eden model.

2. The fractal dimensions and the most important properties of fractal aggregates

Prior to considering some recently proposed, generalised aggregation models, let us give definitions of various fractal dimensions, which are used to describe the growth and properties of fractal aggregates.

The mass fractal dimension, d_f, is the dimensionless exponent in the relationship connecting the number, N, of particles in the aggregate to the linear dimension, R, of the aggregate

$$N = k_0 \left(\frac{R}{a}\right)^{d_f}. \quad (1)$$

The coefficient k_0 is called the prefactor, the structure factor or the first-order lacunarity and a is the size of the primary particles. Usually, the role of linear dimension is played by the radius of gyration, R_g, of the aggregate, which is given by

$$R_g^2 = \frac{1}{N} \sum_{i=1}^{N} (\boldsymbol{r}_i - \boldsymbol{r}_0)^2, \quad (2)$$

where $\boldsymbol{r}_i$ and $\boldsymbol{r}_0$ are the coordinates of the ith particle and the centre of mass of the aggregate, respectively.

The fractal dimension of aggregates grown in numerical simulation is determined using relation (1). This requires preliminary generation of clusters of different sizes followed by plotting of the logarithm of the number of particles *vs.* the logarithm of the radius of gyration, R_g; the slope of this dependence equals the fractal dimension.

The mass fractal dimensions determined for the main models of particle aggregation (see above) are listed in Table 1. As can be

Table 1. The fractal dimensions of aggregates obtained by numerical simulation of cluster growth.[12, 19]

d	Particle–cluster aggregation	Cluster–cluster aggregation
Diffusion-limited aggregation		
2	1.71	1.45
3	2.50	1.80
Ballistic aggregation		
2	2.0	1.55
3	3.0	1.95
Reaction-limited aggregation		
2	2.0	1.61
3	3.0	2.09

seen, the fractal dimension strongly depends on the dimension, d, of the space in which the aggregate was grown and on the aggregation regime. Hereafter we will use the values listed in Table 1 as references in comparing the results obtained using different models.

The mass fractal dimension is sufficient for characterisation of the properties of nearly spherical aggregates. In some systems, particle aggregates possess pronounced shape anisotropy. They are called self-affine aggregates rather than self-similar ones [8] and can be described by two (longitudinal, d_l, and transverse, d_t) fractal dimensions given by

$$N = k_L\left(\frac{L}{a}\right)^{d_l}, \qquad (3)$$

$$N = k_W\left(\frac{W}{a}\right)^{d_t},$$

where k_L and k_W are the corresponding prefactors and L and W are the longitudinal and transverse linear dimensions of the aggregate, respectively.

When considering anisotropic fractal aggregates, the averaged mass fractal dimension is also used

$$\langle N\rangle = k_M\left[\frac{(LW)^{1/2}}{a}\right]^{d_f}. \qquad (4)$$

where the angle brackets denote the averaging over all aggregates characterised by the given length and transverse linear dimension and k_M is the effective prefactor.

Self-affinity of aggregates means that they are invariant with respect to expansion or contraction with different factors, Λ_L, Λ_W, for the longitudinal and transverse linear dimensions, respectively

$$L' = \Lambda_L L,$$

$$W' = \Lambda_W W.$$

By expressing the self-affinity coefficient in the form

$$A = \frac{\ln \Lambda_W}{\ln \Lambda_L},$$

it is possible to interrelate the three fractal dimensions mentioned above

$$d_l = \left(\frac{1+A}{2}\right)d_f, \qquad (5)$$

$$d_t = \left(\frac{1+A}{2A}\right)d_f.$$

Introduction of the trajectory dimension, d_w, of the particles involved in the formation of aggregates (the random walk dimension) appeared to be useful for theoretical analysis. In the DLA regime, particles and clusters experience Brownian motion; the trajectory dimension for a Brownian particle is known [12] to be 2; therefore, $d_w = 2$. Ballistic aggregation is characterised by the motion of particles and aggregates along linear trajectories; hence, $d_w = 1$. For the reaction-limited regime of aggregation, the character of particles motion is of no significance, because particles experience multiple collisions before being added to aggregates and can therefore 'forget' their true trajectories (this holds for all particles). Here, the determining role is played by the point to which the particle or aggregate is attached; therefore, the trajectory dimension for the RLA regime is taken to be zero.

Many properties of fractal aggregates, which will be discussed below, are determined not only by the fractal dimension but also by the so-called chemical dimension, d_c, which is introduced as follows. Let R_c be the minimum distance, which should be travelled to pass from the particle i to the particle j without leaving the aggregate. Let a sphere B_c centred at the particle i be a set of particles j of the aggregate, for which $R_c \leqslant R_0$. Then, the number of particles belonging to B_c increases with increasing R_0 as follows

$$N_c \propto R_0^{d_c}. \qquad (6)$$

which gives the chemical dimension of the fractal aggregate.

The growth laws of irregular fractals are to a great extent dependent on the conditions for penetration of particles into these structures. For instance, growth of a cluster in the DLA regime depends on the ability of a randomly walking particle to reach a particular site. If the sites on the surface of clusters are ascribed some 'masses' proportional to the probability of attachment of a randomly walking particle, it is possible to introduce a new fractal dimension (harmonic fractal dimension d_h) using the dependence of the total 'mass' on the size of the fractal aggregate. This parameter is of crucial importance for determination of various physicochemical characteristics of fractal objects. In particular, knowledge of the distribution of sites possessing activity towards the walking particle is of great importance in studies of adsorption, catalytic reactions, breakdown of dielectrics and dissolution processes.

In contrast to the fractal dimension and chemical dimension, which can be determined using relationships (1) and (6) immediately after aggregation, calculations of the harmonic dimension require either special computations or additional simulation. This parameter can be found by, *e.g.*, solving the Laplace equation for the potential distribution in the space outside of the aggregate at a given surface potential. In this case, the probability of aggregation at a given point is proportional to the surface potential gradient. This problem is too difficult to be solved analytically and therefore the parameter d_h is usually determined using numerical methods.

Meakin [44] reported a study on two-dimensional clusters grown using the Witten–Sander model for diffusion-limited cluster–cluster aggregation and some other models. The clusters were characterised by significantly different fractal dimensions; namely, the d_f values varied from 1.25 to 1.89. The activities of the growth sites were determined using the probe particles experiencing Brownian motion, *viz.*, the growth probability was assumed to be proportional to the number of contacts between Brownian particles and a given site. It was found that d_h has nearly the same value of 0.925 for all the systems studied. This is in agreement with the analytically predicted value $d_h = 1$ for all two-dimensional objects.[45] Grassberger [45] also introduced yet another fractal dimension, namely, the ballistic fractal dimension (d_b), which is determined analogously to the harmonic fractal dimension except that the probe particles are assumed to follow linear trajectories. Unlike the harmonic fractal dimension, d_b strongly depends on the nature of the fractal aggregate.

Generally, the surface of a fractal aggregate requires an infinite hierarchy of fractal dimensions for complete character-

isation,[46,47] which corresponds to the so-called multifractal description of fractal objects (see Section IV). Moreover, an infinite hierarchy of fractal dimensions also arises[47] for those non-fractal surfaces which are characterised by a constant fractal dimension in a particular portion of the distribution curve.

Concluding this subsection, we will give some simple relationships, which characterise the properties of fractal aggregates.‡

The dependence (1) corresponds to the following radial density distribution in a fractal aggregate

$$\rho(r) \propto r^{d_f-d}, \tag{7}$$

where r is the distance from the centre of the aggregate.

The density distribution of the number of particles in aggregates is usually characterised by the density correlation function

$$C(r) = \frac{\langle \rho(r)\rho(0)\rangle}{\rho(0)^2} \propto r^{d_f-d}, \tag{8}$$

where the angle brackets denote the averaging over different orientation of the aggregate. It should be noted that this form of the correlation function is independent of the choice of the origin of coordinates. Namely, if the origin of coordinates is at any point in the cluster, including a point that is well off its centre, the density correlation function decreases obeying the relation (8). Any change in position of the origin of coordinates will affect only the coefficient on the right of expression (8) rather than the exponent. This property of the structure of fractal aggregates was tested by numerical simulation of clusters grown in the DLA regime.[48] As will be shown below, this property is responsible for many peculiarities of the physicochemical properties of fractal aggregates.

Running somewhat ahead, mention may be made that the correlation function (8) corresponds to the intensity of small-angle scattering of electromagnetic radiation by fractal aggregates given by

$$I(q) \propto q^{-d_f}, \tag{9}$$

where q is the magnitude of the scattering vector

$$q = \frac{4\pi}{\lambda}\sin\frac{\theta}{2},$$

and λ is the radiation wavelength and θ is the scattering angle. The scattering intensity obeys the relation (9) at

$$qR_g \gg 1 \text{ and } qa \ll 1.$$

Some generalisations will be considered below.

Using relationships (7) and (8) implies an infinite cluster. However, both real and numerical experiments deal with finite clusters. Because of this, the so-called cutoff function is introduced into relations of the types (7) and (8). For instance, the cutoff function $h(r)$ can be introduced into the density correlation function of an aggregate as follows

$$C(r) \propto r^{d_f-d} h\left(\frac{r}{R}\right). \tag{10}$$

The function $h(r)$ must satisfy the following conditions

$$h\left(\frac{r}{R}\right) \approx 1, \quad r < R, \tag{11}$$

$$h\left(\frac{r}{R}\right) \to 0, \quad r > R.$$

‡ It would be more appropriate to introduce these relationships later but they are necessary for considering the results of some studies concerning the subject of this Section of the review.

In order for fractal dependence of the correlation function on the distance to be valid, the cutoff function should tend to the limiting values faster than power functions.

Knowledge of the cutoff function is required for correct reconstruction of the aggregate size distribution from light scattering data.[49] It should be noted that to a first approximation the introduction of the cutoff function has no effect on the dependence (9). Different cutoff functions were proposed, *e.g.*, an exponent,[50] a stretched exponent[51] and a Gaussian function.[52] A detailed study on the role of the cutoff function in determining the parameters of fractal aggregates has been reported.[53]

3. Generalisations of classical models

Initially, numerical experiments were performed ignoring interparticle interactions. However, real experiments revealed production of clusters whose fractal dimensions differed from those predicted by simple DLA and RLA models. This was explained by specific features of interparticle forces. Therefore, a number of specific experiments and numerical simulation with inclusion of interparticle forces were carried out. The effect of the dipole–dipole interaction on the structure of fractal aggregates grown in the diffusion-limited cluster–cluster aggregation regime was studied.[54,55] Taking the three-dimensional system as an example, it was shown that the d_f value gradually varies from 1.78 for weak to 1.35 for strong dipole–dipole interactions. The fractal dimensions obtained were in good agreement with the experimental values.[56,57]

The effect of the interparticle interaction on the structures of aggregates growing in the reaction-limited cluster–cluster aggregation regime was studied.[58–63] It was found that the structures and the fractal dimensions of the aggregates depend on the particular form of the interparticle interaction. The fractal dimensions obtained were both greater and smaller than the values determined using the classical models.

It should be noted that restructuring of fractal aggregates, which were preliminarily grown using the classical approaches, also allows the aggregates characterised by greater fractal dimensions (compared to the classical values) to be obtained.[60,61]

Diffusion-limited aggregation of particles of different kinds was studied.[64,65] Only particles of different types could bind to each other in a two-species DLA model,[65] which revealed a specific type of percolation transition. Namely, only finite clusters can grow in the system if the fraction of particles of one sort is small, whereas infinite clusters can grow only if the fractions of particles of each sort exceed some critical values.

The Eden model was generalised[66] by introducing an additional internal degree of freedom of the particles, the spin. The model assumes a cluster growing in an external magnetic field and the spin–spin interaction between the nearest neighbours. The new model allows two new fractal dimensions characterising particles with different spin orientations to be introduced. It appeared that the fractal dimension is a nonmonotonic function of the parameter characterising the energy of the interparticle interaction. At low and high interaction energies, the fractal dimension approaches the space dimension and passes through a minimum (the minimum d_f value is 1.79) at intermediate energies of the interparticle interaction. At these energies, the aggregation regime changes in such a way that the cluster structure becomes highly porous. The cluster grown at high energies of the interparticle interaction is characterised by a structure with uniform porosity.

The growth of fractal aggregates near surfaces of various nature was studied by numerical simulation.[67–69] In all cases, aggregates grown in the presence of steric hindrances were characterised by reduced fractal dimensions.

Generalisations of the ballistic model were reported.[70,71] The effects of biases of the trajectories of the particles following streamlines in the viscous fluid near the growing aggregate[70] and accretion of particles on seeds of different (finite) sizes were included.[71]

In most of the above-mentioned studies on the growth of fractal aggregates they were simulated using ensembles of monodisperse particles. Studies on the influence of particle polydispersity on the structure and fractal dimension of aggregates [34, 72–76] revealed that polydispersity has little effect on the fractal dimension even for an ensemble characterised by polymodal size distribution.[76] However, the local structure of aggregates can significantly change, thus affecting the calculated intensity of small-angle light scattering.[75, 76] The cutoff function, which includes the finite size of aggregates, weakly depends on the degree of polydispersity.

4. Analytical models of aggregation

Most theoretical studies on the growth of fractal aggregates involve numerical simulation. There is only a few analytical models of the growth of fractal structures. The reason is the complexity of description of the fractal structure using analytical functions. The most interesting results obtained in this field are briefly outlined below.

Based on general considerations, without using any hypotheses of the structure of aggregates grown in the DLA regime of particle aggregation, it was established [77] that the largest separation between the centre and the most distant point of the aggregate cannot exceed $C_2N^{2/3}$ for the two-dimensional space and $C_dN^{2/d}$ for the spaces characterised by greater dimensions ($d > 2$), where C_2 and C_d are constants. In fact, these relationships place limits on the growth rate of fractal aggregates. It was pointed out that some of the models proposed earlier predicted a faster increase in the aggregate size.

Formation of fractal aggregates in the DLA regime was also studied [78, 79] using an approach which is similar to the Flory model for polymer molecules (see Ref. 80). The authors introduced the effective free energies of repulsion between and attraction of the aggregating particles. An equation for the fractal dimension of the growing aggregates was derived from the condition for the free energy minimum. If an aggregate was grown on the substrate with the dimension $d-m$ in the space with the dimension d, the d_f value for the aggregate is given by [78]

$$d_f = \frac{d^2+1}{d+1} - (d-m). \tag{12}$$

The fractal dimensions found using this relationship are in good agreement with the results of numerical simulation for the spaces and substrates of various dimensions.

The fractal dimensions of aggregates were also analytically determined [81, 82] using the renormalisation group approach (see, *e.g.*, Ref. 83). In this case, the fractal dimension is determined from some recurrent relations rather than from an explicit expression. The fractal dimensions of aggregates thus obtained were also consistent with the values found by numerical simulation.

Sander *et al.* [84] treated diffusion-limited aggregation as a deterministic process of propagation of the interface due to particle diffusion. In this case, calculations of the cluster's growth were reduced to the solution of the Laplace equation with the corresponding boundary conditions. It should be noted that processes of electrochemical deposition, viscous fluid flow in porous media and the breakdown of dielectrics [85, 86] are described by similar equations. Numerical solution of the equations derived showed that the front propagation is accompanied by the development of perturbations on the initially smooth surface, thus resulting in the formation of a dendritic structure. The fractal dimensions of the dendrites growing in two-dimensional and three-dimensional systems were in agreement with the fractal dimensions determined by numerical simulation.

This method of simulation of the growth of dendritic structures has been intensively developed over a long period. Not only theoretical studies but also model experiments have been carried out. The initial model was generalised [87–90] with inclusion of various effects including the anisotropy of transport coefficients near the interface. Theoretical studies on the morphological stability of the growing dendritic structure were also reported.[91–93] It was found [94] that the growing dendritic structures can be characterised by both periodic and random distributions of the secondary branches grown on the primary branch; doubling of the distance between the secondary branches is also possible. The change in the dendrite growth scenario was observed in model experiments. Studies on the growth of ammonium chloride crystals in agar gel revealed [95] that growth of fractal structures instead of crystals with smooth surfaces begins at particular supersaturations. This was explained by surface reconstruction of the growing face under the action of solvent. Transition from regular to chaotic branch growth in dendritic clusters was realised [96] in the experiments on quasi-two-dimensional growth of ammonium chloride crystals between two plates in solution at rather high supersaturations.

These investigations were to some extent reviewed in a study [97] concerned with possible morphologies of the growing structures and conditions for transitions between different scenarios of dendrite growth. Current interest in these models is due to the possibility of using them for growth of structures that do not possess isotropic symmetry (the so-called chiral structures).[98, 99]

Qualitative analysis of aggregation laws [100, 101] made it possible to derive an explicit expression relating d_f to the space and random walk dimensions with inclusion of incomplete accommodation of particles on the growing cluster

$$d_f = \frac{d^2 + \varepsilon(d_w - 1)}{d + \varepsilon(d_w - 1)}, \tag{13}$$

where ε is the particle accommodation coefficient. This equation was confirmed [102] by Monte Carlo simulation of aggregation under conditions identical to those reported in the studies mentioned above.[100, 101]

An analytical model was proposed, which allows one to follow the evolution of diffusion-limited fractal aggregation.[103] A closed equation was derived for the aggregate density and the concentration of primary particles, which predicted a power-law decrease in the density of the growing aggregate.

This model was extended [104] to the case of incomplete accommodation of particles on the surface of an aggregate, *i.e.*, diffusion-limited aggregation, reaction-limited aggregation and an intermediate regime of aggregation were considered in the framework of a unified model. The equations in the generalised model become somewhat cumbersome but not too complicated. Figure 1 presents the fractal dimension of a three-dimensional aggregate plotted *vs.* the particle accommodation coefficient. As can be seen, the model correctly reproduces the limiting cases. The region corresponding to the inflection in the $d_f(\varepsilon)$ curve has attracted considerable interest. The structures of the aggregates grown under these conditions exhibit two domains, a compact

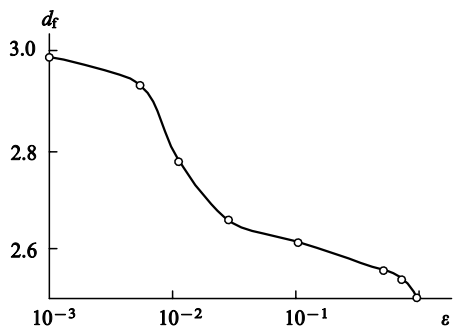


Figure 1. Fractal dimensions of aggregates growing in the DLA regime *vs.* particle accommodation coefficient.[104]

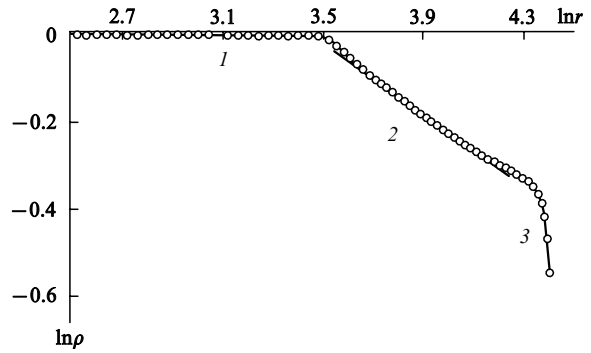


Figure 2. Density distribution for an aggregate grown at intermediate values of the particle accommodation coefficient.
Core (1), fractal shell (2) and peripheral area (3).

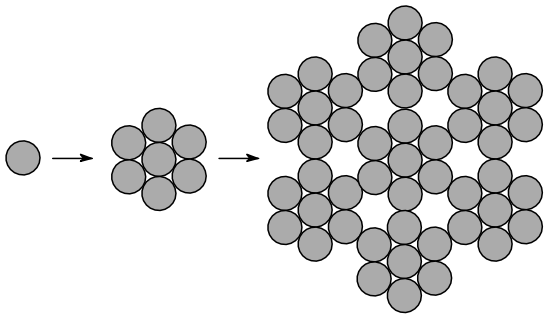


Figure 3. Growth scenario of a self-similar two-dimensional fractal aggregate with the dimension $d_f = \ln 7/\ln 3 \approx 1.77$.

core and a fractal peripheral area (Fig. 2). The presence of two domains indicates that the initial RLA regime is changed by the DLA regime with time. The change in the aggregation regime occurs almost without exception. Therefore, strictly speaking, fractal aggregates should exhibit a multifractal structure (see below).

A model describing the evolution of regularly branched polymers (dendrimers) also belongs to analytical models of fractal aggregation. Dendrimers are synthetic macromolecules with a definite architecture. They can be synthesised by performing repeated reactions.[105–107] Successive 'generations' of branches are built of polyfunctional monomers, emerge from the same centre and form a dendritic structure.

The first theoretical description of the structure of dendrimers was reported by de Gennes and Hervet,[108] though primitive models of such structures were proposed somewhat earlier.[2] Different models of dendrimers were considered in a number of studies [13, 43, 109] and generalised by McCoy.[110] According to the generalised model, a total of Π branches grow at $t = 0$. In contrast to the earlier models, the branches can be characterised by different masses or lengths (some mass distribution of the emerging branches was preset). Then, a total of Π new, smaller branches successively grow at the end of each 'old' branch at regular time intervals. The model assumes that the ratio of the average mass of the new branches, m_i^{av}, to the average mass of the branches grown in the preceding step, m_{i-1}^{av}, is a constant

$$\frac{m_i^{av}}{m_{i-1}^{av}} = \Lambda. \tag{14}$$

In this case, the dendrimer grown is a fractal aggregate with the dimension

$$d_f = \frac{\ln \Pi}{|\ln(\Lambda)|}. \tag{15}$$

As mentioned above, this model is a generalisation of the models proposed earlier. In particular, at $\Pi = 2$ and $\Lambda = 1$, it describes the so-called Cayley tree.[111] The model was used to determine the temporal dependences of the number of branches, the masses and densities of dendrimers and the viscosities of their solutions.

The model of growth of dendritic structures is a particular case of regular models of fractal aggregation. Usually, regular models include some algorithms of generation of self-similar aggregates. One of them is presented in Fig. 3. It is an easy matter to extend this procedure to three-dimensional, self-affine and other aggregates. A comprehensive analysis of regular models of fractal aggregates was reported earlier,[8] so we will not dwell on them here.

Concluding this subsection, mention may be made that thermodynamic characteristics are also suitable for the determination of fractal dimensions of different objects.[112–114] In particular, the fractal characteristics of aggregates were determined using the principle of maximum information entropy production.[113] The size distribution of aggregates was assumed to be lognormal. The fractal dimensions and the standard deviations found using the principle of maximum information entropy production were in agreement with the experimental data.[115]

In most of the models considered above the fractal dimension is governed by the aggregate growth algorithm. Recently, some models have been proposed,[116–119] in which the cluster growth algorithm is prescribed by the fractal dimension and the prefactor in order to provide correspondence between the results of calculations and experimental data. In these models, aggregation occurs by attachment of single particles or fractal aggregates and the position of the attached fragment is preset by the fractal characteristics of the growing system. It can be found with ease using relationships (1) and (2) and the prescribed fractal dimension for both particle–cluster and cluster–cluster aggregations of overlapping and non-overlapping spheres.

5. The prefactor

Quantitative description of clusters using improved experimental methods requires the prefactor k_0 to be determined.[120–123] This coefficient is of particular importance in determining the optical characteristics of clusters (in particular, their scattering power) and their radiating capacities.

Both the prefactor and the fractal dimension can be determined using relationship (1). In contrast to calculations of the fractal dimension, computations of the prefactor initially gave contradictory results. Based on the results of numerical simulation and model experiments, the prefactor was reported to be approximately unity.[121] At the same time, the prefactors measured in studies of soot clusters formed under different regimes of combustion were 1.23 ± 0.07 (see Ref. 120) and 1.66 ± 0.4.[124] Numerical simulation for diffusion-limited cluster–cluster aggregation gave [125] a k_0 value of 1.2 ± 0.15. Analysis of stereoscopic images of soot agglomerates [126, 127] showed that $k_0 \approx 2.4$ and $d_f = 1.64$.

Probably, the reason for the observed differences between the experimental values of k_0 and d_f is an internal rearrangement and partial sintering of aggregates, which, as was mentioned in Refs 128 and 129, predetermine the change in their fractal dimension. An important fact was pointed out:[130] interparticle contacts in real systems should not be treated as point contacts. Hence, one deals with seemingly overlapping particles. Simulation of diffusion-limited cluster–cluster aggregation and processing of the data with inclusion of particle overlap showed that both the fractal dimension and the prefactor increase on increasing the degree of particle overlap (Fig. 4). This dependence can be described by the approximate relationship

$$k_0 = \widetilde{k}_0 \Delta_a^{d_f}, \tag{16}$$

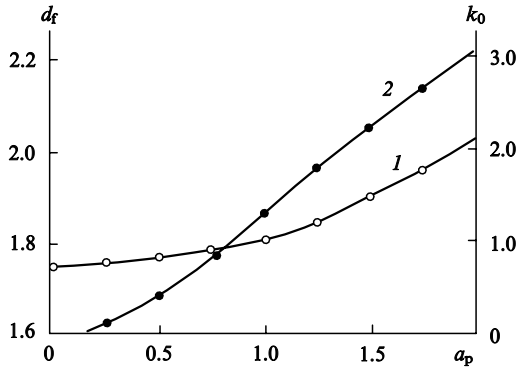


Figure 4. Fractal dimension (*1*) and prefactor (*2*) plotted *vs*. degree of particle overlap (a_p) in a fractal aggregate.[129]

where

$$\Delta_a = \frac{2a}{2a + a_s}$$

(a_s is the distance between the surfaces of the particles) and $\tilde{k}_0$ is the point-contact prefactor.

It was also confirmed [130] that even at $d_f < 2$ the fractal dimension of the two-dimensional projection of a three-dimensional cluster is nearly 10% smaller than the fractal dimension of this cluster only for the point contact case. The inclusion of the monomer overlap increases the discrepancy between the fractal dimensions of the three-dimensional aggregate and its projection.

The assumption of the effect of the degree of particle overlap on the fractal dimension and prefactor was experimentally tested [131] taking the coagulation of polystyrene latex particles with adsorption layers of different thicknesses in different regimes as an example. The fractal dimensions and sizes of aggregates were determined by static and dynamic light scattering, respectively. The results of processing of experimental data confirmed the validity of relationship (16).

III. Kinetics of coagulation of fractal aggregates

1. General relationships

Numerical simulation of the growth of fractal aggregates concerns the structure of aggregates and regularities of changes in their size distribution with time. It was shown [132] that the size distribution, $N_s(t)$, of clusters containing a constant number (s) of primary particles changes with time obeying a self-preserving (or scaling) law

$$N_s(t) \propto s^{-2} f\left[\frac{s}{\langle s\rangle(t)}\right], \tag{17}$$

where $\langle s\rangle(t)$ is the average number of particles in the cluster at instant t, which is given by

$$\langle s\rangle(t) = \left[\sum_{s=1}^{\infty} s^2 N_s(t)\right] \Big/ \left[\sum_{s=1}^{\infty} s N_2(t)\right], \tag{18}$$

and f is some universal function.

Relation (17) for asymptotic cluster size distribution was proposed earlier based on the solution of the Smoluchowski coagulation equation, which in the general case has the form

$$\frac{\partial n_s}{\partial t} = \frac{1}{2}\sum_{i=1}^{s-1} Z(i, s-i) n_i n_{s-i} - \sum_{i=1}^{\infty} Z(s,i) n_s n_i + \tag{19}$$
$$+ \sum_{j=1}^{\infty} Y(s,j) n_{s+j} - \frac{1}{2}\sum_{j=1}^{s-1} Y(j, s-j) n_s,$$

where n_s is the concentration of clusters comprised of s primary particles, $Z(i,j)$ is the coagulation kernel and $Y(i,j)$ is the fragmentation kernel.

A more general relation obtained for a number of model aggregation kernels has the form

$$N_s(t) \propto s^{-\vartheta} f\left[\frac{s}{\langle s\rangle(t)}\right], \tag{20}$$

where $\vartheta = 2$ for systems characterised by conservation of the total mass.

The aggregation kinetics described by the Smoluchowski equation (19) is governed by the forms of the coagulation and fragmentation kernels (detailed analysis of the solutions to the Smoluchowski equation was reported earlier [133]). A classification of uniform coagulation kernels was proposed,[134] which is based on comparison of the probabilities of coagulation of large clusters and of large and small clusters. Depending on which process prevails, it is possible to obtain different laws of aggregation and different cluster size distributions. If aggregation of large and small clusters predominates, no considerable changes in the masses of clusters occur and the size distribution curve becomes bell-shaped. If the interaction of large clusters dominates, small clusters are not involved in the 'battle' and the size distribution curve corresponds to a monotonically decreasing power function.

Two parameters, μ and ν, are responsible for different regimes of growth of the coagulation kernels with increasing cluster size. Namely, $Z(j,j) \propto j^{\mu}$ for large aggregates and $S(1,j) \propto j^{\nu}$ for the probability of coagulation of a large aggregate and a small cluster. For the classical Smoluchowski coagulation kernel, $\nu = 1/3$ and $\mu = 0$. For the same coagulation kernel and fractal aggregates, $\nu = 1/d_f$ and $\mu = 0$. It should be noted that the cases $\nu > 1$ and $\mu > 2$ are physically unrealistic. At $\mu > 1$, the Smoluchowski equation predicts that the formation of an infinite cluster takes a finite time (the so-called gel point). At $\mu \leqslant 1$, no gel transition occurs; the formation of an infinite cluster takes an infinitely long time.

At $\mu > \nu$ and $\mu < 1$ (no gel transition), the cluster size distribution curve is described by a decreasing power function

$$N_s \propto s^{-\tau}, \quad \tau = 1 + \mu,$$

(τ is sometimes called the polydispersity index). Under the same conditions, the mass-average molecular mass is described by an increasing power function

$$M_w \propto t^z,$$

$$z = \frac{1}{1 - \mu}.$$

The radius of gyration, R_g, of fractal aggregates changes with time as follows

$$R_g \propto t^{z/d_f}.$$

For diffusion-limited aggregation with the Smoluchowski coagulation kernel ($\mu = 0$) one has

$$R_g \propto t^{1/d_f}. \tag{21}$$

This dependence was confirmed experimentally. For instance, aggregation of silica particles of size 7 nm was studied by static light scattering.[135] The d_f value obtained using relation (21) coincided with the fractal dimension determined in the same study by small-angle light scattering.

If a gel transition is possible ($\nu < 1 < \mu \leqslant 2$), the size distribution of the growing clusters, which are smaller than some characteristic size, is also described by a power function

$$N_s \propto s^{-\tau},$$

$$\tau = \frac{3 + \mu}{2} > 2,$$

Near the gel point, the mass-average mass of the cluster increases as follows

$$M_w \propto |t - t_g|^{-\gamma},$$

where t_g is the gel transition time and

$$\gamma = \frac{1}{1-\mu}.$$

At $\mu < v$, no gel transition occurs, because $v < 1$. In this case, the formation of a broad size distribution is impossible and the size distribution curve has a bell shape.

In a regime, which is intermediate between the regimes mentioned above, where both types of aggregation are equally significant (at $\mu = v \leqslant 1$), no gel transition occurs and the average mass of the cluster increases as follows

$$M_w \propto e^{ct}. \tag{22}$$

Attempts have also been undertaken to obtain an analytical solution to the Smoluchowski coagulation equation for fractal aggregates using some realistic approximations. Coagulation processes are also studied using aerosols. In this case, aggregation can occur in both free-molecular and continuum regimes. The expressions for the coagulation kernels in these two limiting cases are as follows

$$Z(i,j) = \frac{2kT}{3\eta}\left(i^{1/d_f} + j^{1/d_f}\right)\left(\frac{1}{i^{1/d_f}} + \frac{1}{j^{1/d_f}}\right), \tag{23}$$

for the DLA regime and

$$Z(i,j) = \left(\frac{6kT}{m_p}\right)^{1/2}\left(\frac{1}{i} + \frac{1}{j}\right)^{1/2}\left(i^{1/d_f} + j^{1/d_f}\right)^2, \tag{24}$$

for the free-molecular regime, where η is the viscosity of the disperse medium and m_p is the mass of the primary particle.

Correctness of relationship (24) for aerosol particles was the subject of a study [136] and good agreement with the results of numerical simulation was revealed.

Fractal aggregation in the continuum regime using the Smoluchowski equation with the coagulation kernels for DLA was studied.[137, 138] Both analytical [137] (assuming a lognormal cluster size distribution) and numerical [138] solution of the coagulation equation were obtained. The former solution was reproduced by Park *et al.*[139] Figure 5 presents the temporal dependences of particle concentrations. As can be seen, the formation of fractal aggregates causes a faster decrease in the particle concentration; the reciprocal concentration increases linearly with time for different fractal dimensions.

The existence of a self-preserving solution of the Smoluchowski coagulation equation with the coagulation kernels (23) and (24) was confirmed both numerically and analytically.[140] Based on the numerical solution, simple approximate expressions were presented for the self-preserving solution of the Smoluchowski equation.

The possibility for the self-preserving solution of the Smoluchowski equation to exist was also reported [138, 141–144] for the continuum (DLA) and free-molecular regimes of particle aggregation. The results of calculations [141–144] were confirmed by experiments [143] with silicon and silicon nitride aerosol particles. At the same time, numerical calculations [144] showed that no self-preserving solution exists at $\mu > 1$ because of gel transition.

Sintering of particle aggregates [145–147] and other processes related to the effects of surface phenomena [148] or dispersion composition [149] on the kinetics of particle aggregation [148] only slightly affect the possibility of obtaining the self-preserving cluster size distribution.

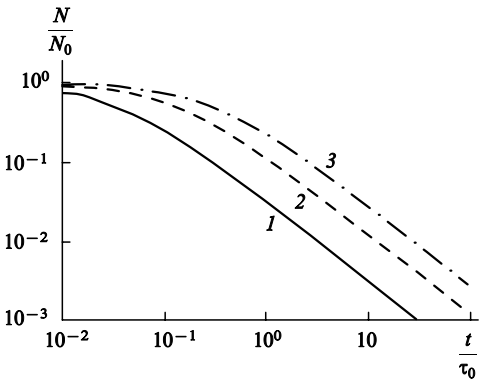


Figure 5. Reduced concentration, N, of aggregates with different fractal dimensions as a function of time.[139]
d_f: 1.5 (*1*), 2.0 (*2*) and 3 (*3*); N_0 is the concentration of primary particles and τ_0 is the half-coagulation time.

2. Coagulation in concentrated dispersions

Recently, considerable attention has been paid to the studies on aggregation in concentrated disperse systems. This is due to advances in computational procedures and to the development of new experimental methods. A feature of concentrated colloidal systems is a significant role of not only the average cluster size and the cluster size distribution but also the structure factor, which is given by (see also the next subsection)

$$S(q) = \frac{1}{N^2}\sum_{j=1}^{N}\sum_{i=1}^{N}\exp[i\boldsymbol{q}(\boldsymbol{r}_i - \boldsymbol{r}_j)], \tag{25}$$

where $\boldsymbol{q}$ is the scattering vector, $\boldsymbol{r}_i$ and $\boldsymbol{r}_j$ are the coordinates of particles and N is the number of particles in the system. The structure factor characterises both long-range and short-range orders in the particle distribution and predetermines the optical properties of dispersions.

Aggregation in concentrated colloidal dispersions can be considered as a stage of phase § decomposition. Phase decomposition in molecular systems is accompanied by definite evolution of the structure factor. Numerous attempts to confirm or reject the validity of these evolutional relations for colloidal systems have been undertaken.

Kolb and Herrmann [150] seem to have been the first to report significant differences between the aggregation in concentrated dispersions and aggregation in strongly dilute colloidal systems. The subject of their study was the numerical simulation of particle aggregation in two- and three-dimensional systems at high concentrations of clusters. The emphasis was placed on the effect of the diffusion coefficient on the structure of the growing aggregates. The diffusion coefficient was assumed to be a power function of the cluster mass. It was found that three types of aggregation can occur in the system at different values of the exponent and initial concentration of particles. These are (i) growth of fractal clusters whose dimensions vary over a wide range, (ii) growth of dense clusters with fractal surfaces and (iii) growth of dense clusters with smooth surfaces. Particular regimes of aggregation allow growth of infinite clusters (*i.e.*, percolation clusters or gel).

Monte Carlo simulation of diffusion-limited cluster–cluster aggregation of colloidal particles in concentrated dispersions was reported.[151] The structure factor was calculated at different instants. The emphasis was placed on verification of the hypothesis of scaling invariance of the dynamical structure factor, according to which

§ The phase state of an ensemble of colloidal particles is kept in mind.

$$S(q,t) = R_g(t)^{d_f} F\left[qR_g(t)\right], \quad (26)$$

where F is a universal scaling function, which does not depend on time in an explicit form. Numerical calculations confirmed the scaling invariance of the dynamical structure factor. At the same time, it was pointed out that some details of the evolution of the colloidal dispersion are different from the model of spinodal decomposition, as was found in the model [152, 153] and numerical [154] experiments. The main difference was attributed to different exponents in the power-law expression for the temporal dependence of the average size of the new-phase domains, namely, the exponent equals 1/3 for spinodal decomposition while depends on the space dimension and on d_f of aggregates for fractal aggregation.

Scaling invariance of the structure factor was the subject of yet another study, numerical simulation of DLA and RLA in three-dimensional space.[155] Using a structure factor similar to that given by (26), the authors tested the validity of the relationship established [156] for spinodal decomposition

$$S(q,t) = q_m^{-3} F\left(\frac{q}{q_m}\right),$$

where $q_m(t)$ is the wave vector corresponding to the maximum value of the structure factor and d is the space dimension (for fractal aggregates, $d = d_f$). The structure factor was also compared with the pair correlation function and it was shown that the peak of the structure factor arises from the correlations between particles belonging to nearest-neighbour clusters. The exponents that relate the position and the height of the maximum of $S(q)$ to time differ from the spinodal decomposition exponents. Though the $S(q)$ for RLA exhibits no peak at short times, eventually its maximum becomes higher than that for the DLA regime. The final shape of $S(q)$ corresponds to a close packing of the clusters after gelation.

A numerical study on diffusion-limited aggregation in two-dimensional colloidal dispersions of various concentrations was also reported by van Garderen *et al.*[157] Conditions for gel transition in the system were established (see Section VI). In the gel state, the system contains a domain of size $r < \xi$ (ξ is the so-called correlation length, which characterises the spatial range of fractal properties of aggregates). At long length scales, the system is a homogeneous medium. The fractal dimension of the grown aggregates coincided with that found for diffusion-limited cluster–cluster aggregation. Variation of the concentration of primary particles affects only the parameter ξ.

The results obtained for three-dimensional systems were somewhat different.[158] The existence of two domains characterised by different length scales, $r < \xi$ and $r > \xi$, was also pointed out. At short length scales, the system has a fractal structure, while at long length scales, the system is a homogeneous medium. However, an increase in the fractal dimension of aggregates with increasing concentration of primary particles was reported, which contradicts the results of this study by van Garderen *et al.*[157] To eliminate the contradiction, a thorough study of aggregation of colloidal particles in dispersions of different concentrations was carried out.[159] Calculations for the three-dimensional space using the diffusion-limited and reaction-limited cluster–cluster aggregation models with inclusion of the dependence of the particle diffusion coefficient on the particle size showed that for both models the fractal dimension increases with increasing concentration of primary particles. This increase for the DLA and RLA regimes can be approximated by the corresponding relationships

$$d_f = 1.80 + 0.91\varphi^{0.51}, \quad (27)$$

$$d_f = 2.1 + 0.47\varphi^{0.66},$$

where φ is the volume fraction of particles. The cluster size increases as a power function of time for DLA and exponentially for RLA. The exponent in the former case and the coefficient in the exponential expression in the latter case are also functions of the initial particle concentration. In both cases, self-preserving cluster size distributions were found, which correspond to the above-mentioned relations (20) with a bell-shaped function $f(x)$ for DLA. The corresponding function $f(x)$ for RLA has the form

$$f(x) \propto x^{-\tau}\tilde{f}(x), \quad \tau = 1.5.$$

Diffusion-limited aggregation in concentrated dispersions was analysed [160] by analytical methods using the known mean-field approximation model.[161] The conditions for cluster formation and the cluster–cluster correlations were analysed with inclusion of the presence of domains with reduced concentrations of particles (monomers). The temporal evolution of the mean cluster radius coincided with that predicted by solution of the Smoluchowski equation. The angular dependences of the scattering light intensities by dispersions were calculated at different instants. Differences between the light scattering by dispersions characterised by the growth of dense and fractal clusters were pointed out. Model experiments showed that scaling invariance of the type (26) during the whole aggregation process is characteristic only of the scattering intensity calculated for the dispersions of dense clusters. The absence of scaling invariance for fractal clusters was explained by differences between the characteristic times of aggregation and of local changes in the concentration of monomers; namely, aggregation is governed by the fractal dimension while the formation of domains with reduced concentrations of particles (monomers) is governed by the space dimension. Scaling-invariant changes in the scattering intensity can occur only immediately prior to gelation.

3. Systems characterised by fragmentation and rearrangement of aggregates

In most cases, numerical experiments concerning fractal aggregation imply rather strong interparticle interactions. In fact, fragmentation of particles is possible, in particular, because of thermal motion. It was Kolb [162] who pioneered numerical experiments on the growth of fractal aggregates by fragmentation. The inclusion of the possibility of cluster fragmentation can lead to an increase in the fractal dimension of aggregates. For instance, d_f increases from 1.78 in the absence of fragmentation to 2.03 if one assumes a low probability of interparticle bond breaking. An increase in the fractal dimension is readily explicable: most often, aggregates comprising fragments connected through a small number of bonds (*i.e.*, the loosest aggregates) undergo fragmentation. Of course, fragmentation of aggregates produces some mass distribution, but the average cluster mass has a finite value.

The effect of bond energy on the fractal dimension of aggregates grown in the diffusion-limited cluster–cluster aggregation regime was studied.[163] Using the two-dimensional model, it was shown that the fractal dimension strongly depends on the bond energy of the particles in the aggregate.

If the homogeneous coagulation and fragmentation kernels meet the conditions

$$Z(\Lambda i, \Lambda j) = \Lambda^{\nu_z} Z(i,j), \quad (28)$$

$$Y(\Lambda i, \Lambda j) = \Lambda^{\nu_y} Y(i,j),$$

where ν_z and ν_y are the homogeneity exponents, the average number of particles in the aggregate is given by [164]

$$\langle s \rangle \propto \left(\frac{Z_0}{Y_0}\right)^{1/(2+\nu_y-\nu_z)}, \quad (29)$$

where Z_0 and Y_0 are the dimensional coagulation and fragmentation constants, respectively,

$$Z(i,j) = Z_0\tilde{Z}(i,j),$$

$$Y(i,j) = Y_0\tilde{Y}(i,j).$$

Here $\widetilde{Z}(i,j)$, $\widetilde{Y}(i,j)$ are dimensionless functions [usually, $\widetilde{Z}(1,1) = \widetilde{Y}(1,1) = 1$].

Dimensional relationships (28) and (29) were used to establish the dependence of the average number of particles in aggregates, their average size ($\langle R \rangle$) and concentration (n) on the volume fraction, φ, of particles in the system.[165] A criterion for gel transition in the system was also proposed.

The growth of fractal clusters, which can undergo fragmentation induced by thermal motion, and gel transition in two- and three-dimensional systems was studied.[166–170] The structure factor $S(q,t)$ of aggregates grown in the diffusion-limited cluster–cluster aggregation regime was determined at different instants by numerical simulation.[166] The height of the maximum of $S(q,t)$ is plotted *vs*. time in Fig. 6. Three main regions in the plot can be pointed out. At short times, the height of the maximum slowly increases [the lower the bond energy, the slower the growth of $S(q_m)$]. At intermediate times, the $S(q_m)$ increases as a power function of time. The duration of this stage is limited by the gel transition, which corresponds to the next, final, stage of the change in the structure factor $S(q_m)$. Here, the $S(q_m)$ slowly increases and reaches a plateau. The higher the bond energy, the slower the increase in the $S(q_m)$. At low bond energies, the plot exhibits no saturation. In this case, the system's behaviour corresponds to the classical pattern for ageing colloidal dispersions, which are characterised by a gradual increase in the size of compact 'droplets' (gel state will be considered in more detail in Section V).

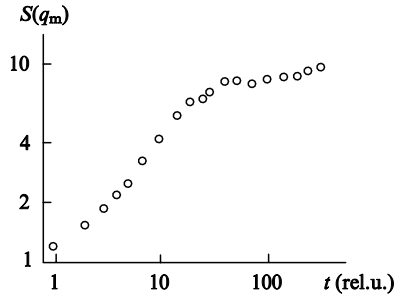


Figure 6. Maximum value of the structure factor, $S(q_m)$, as a function of time for a system of gel-forming aggregates.[166]

Concluding this Section, mention may be made of a number of studies concerning the fragmentation of fractal aggregates by different mechanisms. Etching studies of fractal and non-fractal clusters revealed [171] that the temporal dependence of the number of fragments passes through a maximum and that the number of fragments and the width of their distribution at maximum exhibit power-law dependences on the mass of the initial cluster and on the average coordination number of particles in the cluster. The corresponding exponents depend on the space dimension, starting geometry of the system and on the temperature (the bond breaking probability was assumed to be proportional to the Boltzmann factor). Simulation of etching of fractal objects (aggregates, surfaces and a porous medium) was carried out [172] for both reaction-limited and diffusion-limited regimes. Each object under study was characterised by its own kinetics of etching, governed by the fractal dimension. For instance, the mass of a fractal cluster M decreases with time as follows

$$M \sim (1 - Kt)^{d_f},$$

while the area of the fractal surface obeys the t^{1-d_f} law. It should be noted that fragmentation of fractal aggregates is similar to fragmentation of percolation clusters, which are known to have a fractal structure. Studies on the fragmentation probability of a percolation cluster *via* random rupture of a finite number of bonds have been reported.[173–177] It was shown that fragmentation of such a cluster obeys some scaling relationships; however, they cannot be used in fragmentation studies of conventional fractal aggregates and are therefore not presented here.

IV. Multifractal analysis of fractal aggregates

Some fractal objects cannot be described by one fractal dimension,[178, 179] so one should introduce a large number of parameters similar to the fractal dimension. In this case, the object under study is said to possess multifractal properties.

Often, the question arises as to the multifractal characteristics. For instance, a study on the motion of a fractal aggregate in viscous fluid showed [180] that the distribution of viscous forces applied to particles obeys multifractal relations. It was pointed out [181] that the multifractal approach should be used when analysing the voltage drop distribution at the interparticle contacts in a composite material characterised by near-percolation concentration of the conducting phase. This methodology was also used to study the crack structure distribution in solids [181] and the fluid flow distribution in a porous medium.[182]

Let us consider the multifractal characteristics in more detail. We will examine a fractal object following a conventional formalism by tiling the space of the object into small boxes. Let any box have a unit mass. This allows the mass, M, and the density of the object of linear dimension L to be determined

$$\rho = \frac{M}{L^d}.$$

An increase in the linear dimension of the object by a factor of Λ causes the mass to increase by a factor of Λ^{d_f} and the density to decrease by a factor of Λ^{d_f-d}. Generally, we can write

$$M \sim L^{d_f}, \quad \rho \sim L^{d_f-d}.$$

Since all boxes have equal masses, the changes in the characteristics of the object, which are due to the change in its linear dimension, can be described using one parameter, namely, the fractal dimension d_f. Such an 'equality' of the masses (or other characteristics) of boxes not necessarily corresponds to the physical essence of the object under study. In the example considered above (see Section II), the characteristics of the perimeter of the growing cluster were determined with inclusion of the attachment probability of a new particle to a certain perimeter site. It was shown that different perimeter sites are characterised by different attachment probabilities p. Therefore, it is possible to introduce a probability distribution, $n(p)$, for different perimeter sites. In this way, other elements of the fractal object can also be described by some probability distributions. Like any other probability distribution, the distribution $n(p)$ can be characterised by moments of the order q ¶

$$Z(q) = \sum_p n(p)p^q = \sum_i p_i^q. \tag{30}$$

Summation in the first sum is performed over the probabilities while summation in the second sum is performed over all the perimeter sites characterised by the corresponding probabilities.

Any parameter suitable for quantitative comparison of different regions of a fractal object can be used instead of the probability. Often, the parameters p_i are meant as generalised measures. Examples of the normalised quantities (measures) will be presented below.

Fractal objects belong to the so-called critical structures. According to the theory of critical phenomena, the probability

¶ Literal designation of the moments as q is commonly accepted in the literature. Here, it should be recalled that the letter 'q' has already been used in the review for notation of another quantity (see above).

distribution must be characterised by two critical indices only.[183] This means that it is impossible to obtain additional information on the system by examining the higher moments, because the $(q + 1)$th moment is determined by the exponent, which is found from the qth moment, and some increment Δ. Let the moment be related to the linear dimension L by a power dependence with the exponent $\tau(q)$

$$Z(q) \sim L^{-\tau(q)}. \tag{31}$$

Then, $\tau(q)$ must be a linear function because only two numbers (critical indices) are required to find the dependence $\tau(q)$ (see above). Both numerical simulation and model experiments on many real fractal objects revealed that in the general case the relation between τ and q significantly differs from a linear dependence, which points to multifractality of these objects.

The generalised fractal dimension, D_q (more rigorously, the dimension spectrum), is given by the following relationship

$$(q-1)D_q = \tau(q). \tag{32}$$

As can be seen, $\tau(q)$ equals zero at $q = 1$.

Usually, yet another two characteristics are introduced. These are the so-called Hölder exponent

$$\alpha_m = \frac{d\tau}{dq}, \tag{33}$$

and the Legendre transformation of the function $\tau(q)$, or the multifractal spectrum

$$f(\alpha_m) = q\alpha_m - \tau(q). \tag{34}$$

For true fractal structures, this difference and the parameter D_q are constants.

The physical meaning of these characteristics can be understood taking the aggregation problem as an example. Assuming that the probability of particle attachment to some site changes with the change in the linear dimension of the aggregate (namely, decreases because of the lengthening of the perimeter) as follows

$$p \sim L^{\alpha_m}, \tag{35}$$

from relations (30), (32) and (34) the probability distribution density is given by

$$n(p) \sim C(\alpha_m)L^{f(\alpha_m)}, \tag{36}$$

where $C(\alpha_m)$ is a function independent of the length scale.

When analysing real objects using the multifractal approach, a number of characteristic parameters corresponding to $q = -\infty$, 0, 1 and $+\infty$ are usually considered. At $q \to \infty$, the parameter $\tau(q)$ equals the proportion of the multifractal set, which is characterised by the highest probability, and D_∞ equals the minimum α_m value for the system in hand. And *vice versa*, at $q \to -\infty$, $\tau(q)$ equals the proportion of the multifractal set, which is characterised by the lowest probability, and $D_{-\infty}$ equals the maximum α_m value. At $q = 0$, the parameter D_0, which is equal to the maximum value of the function $f(\alpha_m)$, characterises the dimension of the measure carrier (*i.e.*, the multifractal object itself). For a monofractal object, D_0 equals the fractal dimension of the object. Finally, at $q = 1$, the parameter D_1 is equal to the dimension of information entropy (generally, it can be considered equal to the dimension of the generalised Renyi entropy).

Typical dependences $D_q(q)$ and $f(\alpha_m)$ are shown in Figs 7 and 8. Real systems can exhibit marked deviations from these dependences.

There is an analogy between the multifractal and thermodynamic formalisms. Let us re-write relationship (30) in the form

$$Z(q) = \sum_p e^{F(p)}, \tag{37}$$

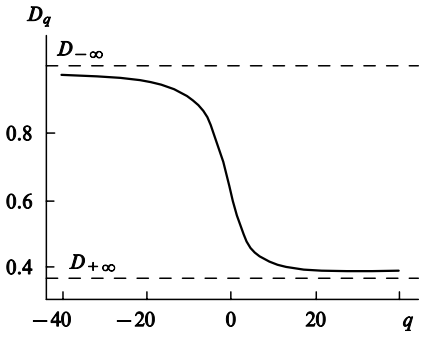


Figure 7. Typical fractal dimension spectrum.[180]

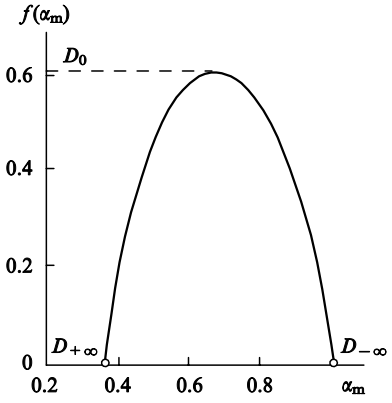


Figure 8. Typical multifractal spectrum and its characteristic points.[180]

where $F(p) = \ln n(p) + q\ln p$. Suppose that the major contribution to the sum on the right of Eqn (37) comes from the terms with $p = p^*$, where p^* corresponds to the maximum value of the function under the summation sign. Then one gets

$$Z(q) \approx e^{F(p^*)} \propto L^{\tau(q)} = L^{f(\alpha_m)-\alpha_m q}. \tag{38}$$

As can be seen, the function $Z(q)$ formally plays the role of the statistical sum of the thermodynamic system while $\tau(q)$ is the free energy and q is the reciprocal of the temperature. The Legendre transformation $f(\alpha_m)$ is an analogue of the entropy, the parameter α_m is an analogue of the energy while the dependence $f(\alpha_m)$ is easily recognisable as similar to the relation between the entropy and energy of the thermodynamic system. The analogy between the fractal and thermodynamic formalisms has been the subject of a thorough study.[184]

The multifractal thermodynamic characteristics of the fractal aggregates grown in the DLA regime have been reported.[185] The generalised Renyi entropies were calculated

$$I_q(L) = \frac{1}{q-1}\ln\sum_i p_i^q, \quad q \neq 1, \tag{39}$$

$$I_1(L) = \sum_i p_i \ln p_i,$$

and their changes during the aggregation simulated using the Brownian dynamics approach were followed.

The Renyi entropies depend on the fractal dimension of aggregates. An increase in the number, N, of particles in the aggregate causes the Renyi entropies to increase in proportion to $\ln N$. The coefficient of proportionality,

$$K_q = \frac{I_q}{\ln N}$$

for this dependence is determined by the fractal dimension of the aggregate and the q value. At $q \leqslant 1$, the parameter K_q decreases, while at $q > 1$ it increases on increasing the fractal dimension. This coefficient can be used to determine the degree of multifractality of aggregates, which is defined [186] as the entropy difference between the domains corresponding to the maximum ($q \to +\infty$) and minimum ($q \to -\infty$) measures, *i.e.*, $K_{-\infty}(N) - K_{+\infty}(N)$. According to calculations, this difference tends to zero as the number of particles in the aggregate increases. Thus, transition to a true monofractal is possible in the limit $N \to \infty$; the aggregate comprising a finite number of particles possesses multifractal properties.

An attempt has been undertaken [187] to go beyond the scope of a simple analogy between the multifractal and thermodynamic descriptions. The 'thermodynamic' behaviour of multifractal systems was compared with the thermodynamic behaviour of conventional physical objects. The 'thermodynamics' of multifractals was considered in the constant specific heat approximation. This choice is due to the fact that the specific heats of gases and solids remain constant over a rather wide temperature range. In this approximation, the function f should have the form

$$f(q) = a_{\mathrm{m}} - c_{\mathrm{m}} \ln q, \tag{40}$$

where a_{m} and c_{m} are constants and q is the constant specific heat. For the generalised dimension from Eqn (32) one has

$$D_q = (a_{\mathrm{m}} - c_{\mathrm{m}}) + c_{\mathrm{m}} \frac{\ln q}{q-1}. \tag{41}$$

The dependence $f(q)$ is plotted in Fig. 9. As can be seen, the constant specific heat approximation fits well the results of numerical experiments.

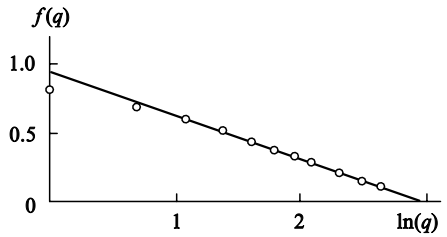


Figure 9. Multifractal spectrum calculated for the DLA regime (points) [188] and calculated in the constant specific heat approximation (straight line).

Analogous dependences for the generalised fractal dimension are presented in Fig. 10. The results of numerical simulation are in good agreement with the fractal dimension spectra obtained in the constant specific heat approximation. Interestingly, the slope ratio of the straight lines in Fig. 10, which is equal to the 'specific heat' ratio, is $\sim 3/2$, as in the case of the specific heats of three- and two-dimensional gases. It has been shown [188] that the constant specific heat approximation describes the multifractal spectra obtained by different authors for various systems (*e.g.*, stress distribution for percolation cluster, surface profile of corroding material, turbulent diffusion, *etc.*).

The multifractal analysis of the clusters growing in the DLA regime showed [190–192] that the clusters are characterised by a more complex structure than could be expected based on the fractal dimension and anisotropy factor only.

Consideration of correlations between the measures of a multifractal object showed [191] that the correlation function has the form

$$\langle p(r')^m p(r'+r)^n \rangle \simeq \left(\frac{R}{a}\right)^{d_{m+n}} \left(\frac{r}{a}\right)^{d_m + d_n - d_{m+n}}, \tag{42}$$

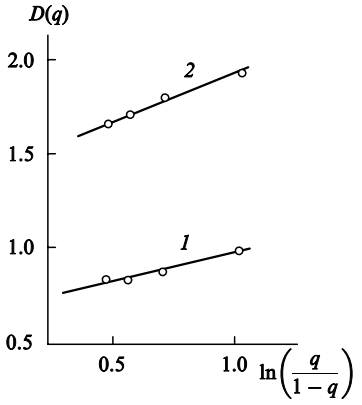


Figure 10. Fractal dimension spectra for two-dimensional (*1*) and three-dimensional (*2*) DLA [189] plotted in the constant specific heat approximation.

where a and R are respectively the lower and the upper bounds of the fractal behaviour of the measure carrier ($a < r < R$; a is the short cutoff and R is the overall radius of the object), $d_q \equiv (1-q)D_q - d_{\mathrm{f}}$ and d_{f} is the fractal dimension of the measure carrier. The existence of a single scaling form over the full range of radius indicates that the multifractal object is a set of blocks similar to those used in polymer physics rather than a superposition of fractal sets.

A similar approach to the description of fractals treats fractal aggregates as sets of 'branches' with certain masses m.[192] For a typical cluster comprised of N particles, the branch mass distribution, $n(m, N)$, was introduced. Processing of a large body of data obtained by numerical simulation of aggregates showed that this distribution obeys the law

$$\frac{n(m,N)}{N} \sim m^{-\beta}. \tag{43}$$

More recently,[193] it was shown that this power law can be derived from the maximum entropy principle. In this case, the entropy is expressed through information necessary for growing a fractal object with prescribed structure and size. Taking a number of fractal objects, which can be grown iteratively, it was demonstrated that the maximum entropy principle allows, on the one hand, the power laws of changes in some characteristics of fractals to be established, and, on the other hand, the fractal dimension to be calculated without determining the spatial structure of fractal objects.

Theoretical conclusions were confirmed by the data of experiments [194] with polystyrene latex particles of size 600 nm, which floated on the surface of aqueous $MgSO_4$ solution. The image of the surface fluid with floating particles was tiled into boxes of a particular size δ. Each box was ascribed a measure p_i equal to the ratio of the number of particles in the box to the total number of particles in the system. The multifractal characteristics can be found with ease from the following expressions

$$\tau(q) = \lim_{\delta \to 0} \frac{\ln \sum_i p_i^q}{\ln \delta}, \tag{44}$$

$$\alpha_{\mathrm{m}}(q) = \lim_{\delta \to 0} \frac{\sum_i \hat{p}_i \ln p_i}{\ln \delta},$$

$$f(q) = \lim_{\delta \to 0} \frac{\sum_i \hat{p}_i \ln \hat{p}_i}{\ln \delta},$$

where

$$\widehat{p}_i = \frac{p_i^q}{\sum_i p_i^q}. \quad (45)$$

The multifractal spectra of aggregating two-dimensional dispersion at different instants are shown in Fig. 11. Some peculiar features should be pointed out. The maximum in the curve is related to the fractal dimension of the measure carrier, *i.e.*, to the fractal dimension of the substrate regions characterised by the nonzero measure. A large number of empty regions is also present in the system in question; because of this, the fractal dimension of the measure carrier is less than two. The information entropy and the fractal dimension of the measure carrier are plotted *vs.* time in Fig. 12. As can be seen, both dimensions decrease with time. This is typical of two-dimensional aggregation of colloidal particles. A decrease in the entropy dimension is explained by a decrease in the monolayer entropy upon aggregation.

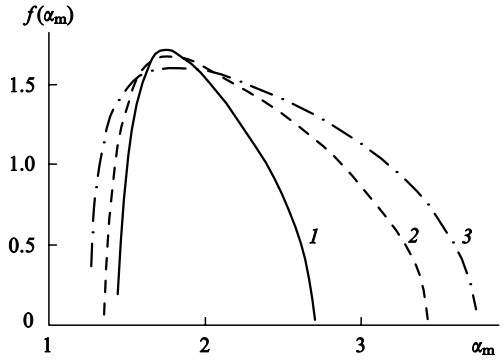


Figure 11. Multifractal spectra of aggregating two-dimensional dispersions at different instants of time.[194]
t /s: 122 (*1*), 613 (*2*) and 2401 (*3*).

Using the relations mentioned above implies an all-scale self-similarity of the object analysed using the multifractal approach. Real objects are self-similar at certain length scales. This means that in the general case the multifractal spectrum depends on the length scale. Taking into account this scaling dependence, it is possible to draw some interesting conclusions concerning the length scales appropriate for multifractal analysis of objects.[195] Let us take an ensemble of particle aggregates as an example and analyse it using the multifractal approach.

Let us tile the entire space into boxes of linear dimension δ. Let the proportion of particles in the box i be the measure p_i. Clearly, the sum of the measures over all boxes equals unity. The average measure in the filled boxes equals the reciprocal of the number of the filled boxes

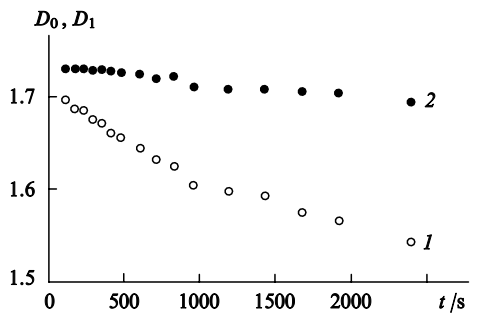


Figure 12. Information entropy (D_0) (*1*) and fractal dimension of the measure carrier (D_1) (*2*) plotted *vs.* time.

$$\langle p \rangle = Z(0,\delta)^{-1}. \quad (46)$$

The dispersion of the measure in the boxes is given by

$$\sigma_p^2 = \langle p^2 \rangle - \langle p \rangle^2 = \frac{Z(2,\delta)}{Z(0,\delta)} - \frac{1}{Z(0,\delta)^2}. \quad (47)$$

For monofractal objects one has

$$Z(0,\delta) \sim \delta^{-d_f},$$

$$Z(2,\delta) \sim \delta^{d_f}.$$

As a result, the measure dispersion remains constant upon changing the box size. For multifractal objects, the first term in Eqn (47) is proportional to $\delta^{D_2+D_0}$ and the second term is proportional to δ^{2D_0}; *i.e.*, the measure dispersion varies with the change in the box size. Therefore, it is possible to find a box size (for a normal multifractal spectrum, where $D_2 < D_0$ on the long length scale, and for an anomalous multifractal spectrum, where $D_2 > D_0$ on the short length scale) such that the measure dispersion becomes equal to zero. Further change in the length scale will not affect the dispersion, because it cannot be negative. So one can say that, from the measure distribution standpoint, the system will be homogeneous beyond the limiting length scales. In the case of colloidal systems the minimum box size nearly equals the particle size or the correlation radius.

Yet another field of application of the multifractal approach is the determination of the fractal dimension of real finite systems. The point is that the use of the relationship given in p. 824 faces some difficulties, because this relation 'works' well only in the case of ideal (in the mathematical sense) fractal objects. Real systems are characterised by finite dimensions, which confines the range of fractal behaviour. Therefore, the fractal dimension is usually estimated rather than calculated. The procedures for reliably estimating the fractal dimension have been discussed in the literature.[196–199] Usually, it is possible to determine several different fractal dimensions. A typical curve for the determination of the fractal dimension of an object, obtained using the box-counting technique, is shown in Fig. 13. The curve degenerates into a straight line only for true fractal object. Otherwise (including multifractal structures), a number of straight-line portions are observed. Usually, region *1* (large δ) characterises the fractal dimension of the space into which fractal objects can be embedded. The slope of the straight line in region *2* (small δ) determines the fractal dimension of the embedded object. Unambiguous interpretation of the intermediate region *3* is impossible, because its pattern is to a great extent determined by the character

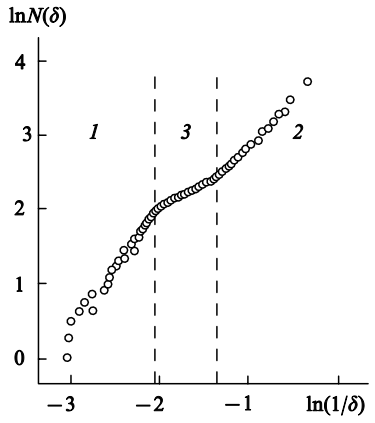


Figure 13. Typical curve for determination of the fractal dimension using the box-counting technique.
(*1–3*) see text.

of the spatial distribution of fractal objects. It can be treated as the region of the fractal dimension distribution, corresponding to the multifractal properties of the system under study.

V. Fractal gels and emulsions

1. Fractal gels

The size of fractal aggregates increases much faster than their mass during the aggregation process. At a certain particle concentration, which is specific to each fractal dimension value, the aggregates grown can fill the entire space, thus forming a gel structure composed of a network of connected clusters. Colloidal diffusion-limited cluster–cluster aggregation in two-dimensional systems was studied using the Smoluchowski coagulation equation [200] and by numerical simulation.[201] The evolution of the cluster size distribution was followed; the gel was treated as an infinite fractal cluster. It was shown [202] that, if the volume fraction of the primary particles exceeds some critical value, φ_c, diffusion-limited cluster–cluster aggregation results in a homogeneous network formed by fractal clusters of size ξ.

There is a large number of models, which describe the transition of colloidal dispersions to the gel state. They are based on the classical fluid theory equations adapted for colloidal systems.[203] The approach employed includes the Brownian dynamics simulation [204–207] with different potentials of interparticle interactions, *e.g.*, the Derjaguin–Landau–Verwey–Overbeek,[204, 205] Lennard-Jones [206] or the depletion potential.[207] The molecular dynamics approach [208] is also employed in the studies of gelation at the molecular level.

The simplest models of gel formation upon particle aggregation usually assume [209] that the fractal dimension of aggregates remains unchanged during their growth under, *e.g.*, the DLA or RLA conditions. The volume fraction of particles in the fractal aggregate can be found with ease from

$$\varphi_a = \left(\frac{R}{a}\right)^{d_f-3}. \tag{48}$$

Gel transition occurs if the volume fraction of particles in the fractal aggregate becomes equal to the volume fraction of clusters in the entire system (at $\varphi_a = \varphi$). All clusters are assumed to have the same mean size $R = \xi$. In this state, there is a region of size $r < \xi$ (see Section III) in the system where the aggregates possess fractal properties. At long length scales, the system is a homogeneous medium whose fractal dimension equals the space dimension. The correlation length, ξ, is determined by the volume fraction of particles and is given by

$$\xi \approx a\varphi^{-1/(3-d_f)}. \tag{49}$$

The simplest model for gel formation can be applied to explain the results of experimental studies on the dynamics of the structure factor of dispersions. Experiments showed [152, 153, 210–214] that, if fractal aggregation in the system results in the formation of a gel, the dependence of the structure factor $S(q,t)$ on the wave vector at different instants passes through a maximum. Small-angle neutron, X-ray, and light scattering studies of a broad class of dispersions (aluminosilicate gels,[210] polystyrene latex particles,[152, 153] polymer gels [211] and monodisperse oil droplets in water [212, 213]) also showed that the position of the maximum, q_m, is inversely proportional to the ξ value at a given instant. This maximum is interpreted as an indication of the transition from the fractal regime of scattering [at intermediate q values corresponding to $S(q) \propto q^{-d_f}$] to the scattering by a homogeneous medium (small q values). It was also established [152, 211, 215] that

$$S(q_m, t) \propto \xi^{d_f}, \tag{50}$$

$$q_m \propto S(q_m,t)^{-1/d_f},$$

$$t_g \propto \varphi^{-d_f/(3-d_f)},$$

where t_g is the gel time.

These relationships were tested in the Monte Carlo studies of gel formation in the diffusion-limited cluster–cluster aggregation regime.[158, 216] It was found that in the short-time scale the cluster size changes as follows

$$\xi \propto \left(\frac{t}{t_g}\right)^{1/d_f}.$$

As time passes, the exponent decreases; it should be noted that the higher the concentration of primary particles in the system, the earlier the decrease begins. The power-law relationship between q_m and $S(q_m,t)$ was confirmed with high accuracy; however, the exponent remained constant on increasing the concentration of primary particles, whereas the fractal dimension of the growing aggregates increased substantially. On this basis, it was assumed that the gelating systems are also characterised by the apparent fractal dimension of aggregates, which governs the relation between q_m and $S(q_m,t)$. A detailed review on the kinetics of formation of fractal gels from colloidal particles was reported by Poon and Haw.[170] They considered the processes of gel formation from colloidal particles and from colloidal particles and polymers and analysed the peculiar features of small-angle light scattering by gels of colloidal particles, which are due to the existence of a mesoscopic fractal structure.

In fact, fractal gels have a more complex structure compared to that predicted by the simplest model and the process of gel formation involves several stages.[208] At first, clusters are formed from monomers and then grow under DLA conditions. The initial gel network is comprised of the largest aggregates and then smaller aggregates and free particles are included. In this stage, intercluster interactions become increasingly significant. Thus, the formation of a gel network is accompanied by slow changes in the structural organisation of particles.[217] Breakage of certain bonds and the formation of new bonds induce restructuring of the gel, which is accompanied by an increase in the dimensions of fractal objects. The multistep process of gel formation in colloidal dispersions was confirmed in a series of experimental studies [218–220] carried out using various methods of analysis of the gel structure, which allowed length scales from several nanometres to 5000 nm to be investigated.

Restructuring of aggregates after formation of a gel network is possible in the systems characterised by rather weak attractive interparticle interactions.[167–170, 221, 222] Here, the lifetime of the gel network can be rather long. However, if the interparticle bonds can be broken, the network is restructured because this state of particles in colloidal systems is metastable compared to gas–liquid phase transitions. Usually, such gels are called transient gels,[223] though in fact all gels of colloidal particles are treated as transient gels (though for some of them the time for transition to the equilibrium state is too long). Numerical simulation of the process of transient gel formation has been the subject of a large number of studies (see, *e.g.*, Refs 205, 206, 222, 224 and 225). Transient gels obey common relations for the pair correlation function, $g(r)$, and the particle density distribution, $n(r)$

$$g(r) = \left(\frac{r}{\xi}\right)^{d_f-3},$$

$$n(r) = n_0\left(\frac{r}{a}\right)^{d_f}$$

(n_0 is the normalising factor) and for the correlation length; however, the parameters of these distributions (including d_f) change with time.

Modern experimental studies are mainly carried out in order to establish a relation between the parameters of gels and

conditions for gel formation. In particular, the effects of the properties of the disperse medium [226, 227] and of the regime of coagulation of the primary particles [226, 228] on the fractal dimensions and correlation lengths of gels have been studied. The range of substances used for the formation of hydrogels is extended [229–233] (here, silica undoubtedly ranks first). New experimental procedures for the determination of the sol–gel transition point, kinetics of fractal aggregation and fractal characteristics of gels are elaborated (*e.g.*, rheological [232, 233] and electrical conductivity methods [234]).

Studies on the dynamics of the restructuring of gels are a particular avenue of experimental research. Here, the main difficulty is due to the low rate of the process. Nevertheless, interesting results have been reported recently.[235] Experiments were carried out with gels of polystyrene latex particles of size 10 nm dispersed in a light/heavy water mixture, which provided neutral buoyancy of particles. The volume fraction of particles varied from 10^{-4} to 10^{-3}. The fractal dimension of the freshly formed gel was 1.82. It was established that the dynamical structure factors of the gels obtained obeys the law

$$S(q,t) \propto \exp\left[-\left(\frac{t}{\tau_f}\right)^{\beta_g}\right], \tag{51}$$

with $\beta_g = 1.5$ and $\tau_f \propto q^{-1}$. Ageing causes the time τ_f to increase substantially. The temporal dependences obtained for different q can be scaled on a single master curve, with τ_f growing linearly with age. It should be noted that the temporal dependence of type (51) was reported earlier [236] for an identical gel of polystyrene latex particles of size 9.5 nm with a somewhat different β_g value (0.66). No changes in the relaxation time were observed, except for a rather strong dependence of this parameter on the concentration of primary particles.

To explain these observations, a model was proposed, which is based on the syneresis of a gel and on its local shrinkage [the case in point is (i) the compaction of fractal fragments and (ii) restructuring of the gel]. The model allows experimental dependences to be reproduced correctly at a qualitative level. Densification of the central part of aggregates was reported in a study [237]on the evolution of gels formed in methylcellulose solutions.

Until recently, gel formation was observed only in liquid dispersions. The first experiment on the formation of gels initially in the gas phase was reported by Lushnikov *et al.*[238] who prepared the so-called fractal wires. The metal surface was exposed to intense laser radiation; subsequent application of a strong external electric field induced the 'growth' of a thick wire formed by fractal clusters attaching to the metal surface. The mechanism of wire formation is rather simple, namely, metal vapours are condensed in the form of nanoparticles which form fractal clusters. The external electric field induces directed aggregation into macroscopic fractal structures. A feature of the process is that the fractal wires at first grow in the gas atmosphere and then are attached to the surface.

Fractal wires from steel, brass and carbon particles have been produced analogously.[239] A thorough examination of the structures showed that the primary particles are 1 to 10 nm in diameter and up to several millimetres long and possessed pronounced anisotropy. The 'lifetime' of the wires reached several weeks at zero electric field between the electrodes. The mechanism of formation of these structures is still to be clarified. The point is that one should take into account not only accelerated coagulation of particles but also their deposition on the electrodes. Here, the main contribution comes from Brownian diffusion of the particles and from their motion in the electric field. The nonuniformity of the electric field should also play a significant role. This is unavoidable in the system under study both at the electrode surfaces covered with the deposits and in the space between the electrodes, filled with rather large and readily polarisable aggregates.

The formation of an aerogel from soot particles formed during acetylene combustion has been studied.[240] The primary particles of size 10 to 30 nm, which are usually formed in flames, grow (most often, under DLA conditions) into fractal aggregates with the radii of gyration varied between 50 and 100 nm. The experiment involved determination of the structure factor and photography of the upper region of the flame at different flow rates of acetylene. Measurements and observations showed that at sufficiently low flow rates of acetylene the structure factor corresponded to the presence of flame fractal aggregates with a dimension of 1.8. At rather high flow rates of acetylene, the dependence of the structure factor on the wave vector exhibits a maximum and some contacting aggregates of size of at most 5 μm are observed in the system. This indicates formation of a flame aerogel. Estimation of the aggregation rate of soot particles showed that it much exceeds that expected from the Smoluchowski equation. The mechanism of accelerated aggregation is also still to be clarified; mention was only made that studies of the sol–gel transition in the liquid phase also revealed [241] accelerated aggregation.

2. Fractal emulsions and microemulsions

In studies of the mechanical properties of aqueous emulsions [242, 243] it was conjectured that their spatial structure is characterised by the presence of inhomogeneous regions possessing the properties of fractals. This was confirmed in a quenching study [244] of the microstructure of silicate glass in a liquid with low glass affinity (fractal properties were observed at a certain fraction of the dispersed phase). The data were analysed based on the concept of the so-called connected cluster, which is similar to a percolation cluster. However, analysis was performed by inclusion of all particles in the entire system, so the total number of particles much exceeded the number of particles in the connected cluster. Therefore, the fractal structure reported in Ref. 244 cannot be explained by effect of this cluster.

The fractal structure of emulsions was also assumed to have a dynamical nature [245] and numerical simulation of a two-dimensional ensemble of disks with short-range attractive interactions was carried out. The type of particle distribution in the system was determined from the relationship between the number of particles in the circle $g(r)$ and the circle size r. For a system of noninteracting particles or at a low energy of interparticle interaction

$$U < kT$$

the particle distribution was uniform. The system with strong interparticle interaction

$$U > 3kT$$

was characterised by the formation of associates followed by separation into two phases. At

$$kT < U < 3kT$$

clustering occurred. The composition of clusters varied with time. The function $g(r)$ for the region occupied by the cluster was found to be a power function with a fractional exponent equal to the fractal dimension of the growing clusters. It was established that the fractal dimension increases on increasing the concentration of disks in the system.

Microemulsions, or surfactant-stabilised, thermodynamically stable homogeneous mixtures of polar (water) and non-polar (oil) liquids, belong to yet another group of colloidal objects with fractal structures. The surfactant molecules are usually distributed over the oil/water interfaces, which confine nanodroplets of water or oil.

Microemulsions are characterised by diverse structural organisations. Here, only three of them will be pointed out. If oil is present in excess, the phase L_2 comprised of water-containing surfactant micelles distributed in oil is usually formed. Otherwise (water-rich compositions), a microemulsion is comprised of surfactant-coated oil droplets dispersed in water (phase L_1). The

presence of water and oil in nearly equal proportions leads to formation of a bicontinuous phase (structure with surfactant-separated interpenetrating domains of the oil and water phases). The phase state of the microemulsions is to a great extent determined by the temperature and salinity of the aqueous solution.

Interestingly, by increasing the water-to-oil ratio it is possible to pass from the phase L_2 to the phase L_1 through the bicontinuous phase. This transition is accompanied by changes in the physicochemical properties of the microemulsion. The most remarkable is a dramatic (by several orders of magnitude) increase in the conductivity of microemulsion, which is usually considered as a percolation transition.[246–249]

Observation of this transition indicates that microdroplets must form a fractal structure corresponding to the percolation cluster.[5] At the same time, treatment of microemulsions in the framework of the fractal approach is seldom the case, though the earlier Monte Carlo simulation [250] revealed fractal aggregation in microemulsions. It is the concept of fractal aggregation that allowed agreement between the theoretical and experimental temperature dependences of the conductivity of microemulsions on the concentration of the conducting phase to be established.

It was shown [251] that dynamic light scattering in microemulsions can be described in terms of the fractal aggregation of microdroplets and that the fractal dimension of the percolation cluster (2.5) is quite appropriate to account for the experimental data. This approach was also used [252] to describe the temperature dependences of the viscosity and elastic modulus of a microemulsion and of the dependences of the ultrasound velocity, specific heat and viscosity on the concentration of droplets. The great potential of the fractal methodology for the theory of microemulsions was confirmed by the results of experiments on the kinetics of quenching of fluorescent probes [253] and diffusion of water molecules,[254] dynamical percolation transitions [255, 256] and fluctuation effects [257] in microemulsions near the percolation threshold. The fractal nature of the structure of microemulsions is also indicated by numerical simulation data and analytical calculations of the dynamics of the processes in the oil/water/surfactant systems during the formation of microemulsions from a (initially) homogeneous ternary mixture.[258–261] This also holds for the interfaces in microemulsions.[262] Thus, application of the fractal approach to such interesting systems as microemulsions offers considerable promise.

VI. Two-dimensional fractal structures

Numerical simulation of aggregation processes usually concerns the laws of aggregation in spaces of different dimensions. The case for two-dimensional space is most often studied. This is mainly due to considerable reduction of computational cost, while the results obtained differ from those typical of the three-dimensional systems only quantitatively. However, interest in two-dimensional systems is not only of theoretical but also practical value. Modern technologies require knowledge of the laws of the interfacial behaviour of colloidal particles. These can be, *e.g.*, the water/air or oil/water interfaces; aggregation of particles at the solid/liquid interface is also possible.

Because of the need for research on aggregation in the two-dimensional space, numerical simulation was followed by experimental studies nearly immediately. It should be noted that such experiments have some advantage over the experiments with three-dimensional systems, namely, the structures of two-dimensional aggregates can be observed immediately using various microscopy techniques without distorting the objects under study.

1. Air/liquid interfaces

The pioneering experimental studies on the laws of fractal aggregation at interfaces were reported by Hurd and Schaefer [263] and Onoda.[264] They used micrometre-sized, hydrophobised particles of silica [263] and polystyrene [264] distributed over the surface of aqueous salt solution. The experiments were carried out under DLA conditions. The values of the fractal dimensions determined appeared to be close to those found from numerical simulation.

There are three main types of interaction between particles trapped at interfaces. These are the electrostatic repulsion, molecular attraction and capillary interaction, which can be both an attractive and repulsive interaction. The electrostatic and capillary forces can be controlled with ease by adding salts in solution and by changing the extent of modification of the particle surface. The possibility of controlling the interaction forces allows the regime of particle aggregation to be varied. In particular, no changes in the structure of aggregates were observed [265–267] upon change in the regime of cluster–cluster aggregation of polystyrene latex particles on the surface of water from DLA to RLA.

Studies on the aggregation of glass beads at the water/octane [268] and water/air [269, 270] interfaces were carried out in different regimes of particle aggregation including those allowing the aggregates to undergo restructuring. Experiments showed that the aggregates can have either a fractal or non-fractal structure depending on the regime of aggregation. The fractal dimension of the growing aggregates depends on the hydrophobicity of the particle surface and on the concentration of salt in solution. Under particular conditions, rather large aggregates are characterised by the internal structure, as indicated by a break in the plot of the logarithm of the cluster density *vs.* distance to the centre of the cluster. The break was ascribed to the action of capillary forces, which contract the soft peripheral area of aggregates (see below). The interior of the large clusters is characterised by the same fractal dimension as the small aggregates. Considerable attention was paid to the restructuring of the grown aggregates. No quantitative relationships were found, but simple estimation showed that restructuring of aggregates is to a great extent controlled by the repulsive electrostatic forces. This conclusion was confirmed in the experiments on aggregation of polystyrene latex particles on the surface of water. In this case, the possibility of restructuring of aggregates was provided by specific adjustment of the parameters of the colloidal system.[271] By varying the electrostatic repulsion between particles it was possible to grow both compact aggregates and two-dimensional 'foam' formed by chains of particles.

A comparison of the laws of aggregation of rod-like and spherical particles at the water/air interface was reported.[272] The experiments were carried out with polydisperse rod-like soot particles 35 μm thick and 140 μm long and monodisperse glass beads 75 μm in diameter with different extent of surface hydrophobicity. The fractal dimension of two-dimensional structures was determined using three methods (box-counting technique, density correlation function and the number of particles–box size correlation). Experiments showed that the shape of particles has no effect on the laws of aggregation because the fractal dimensions of the aggregates of soot particles and of glass beads differed only slightly; at the same time, the fractal dimension of glass beads was affected by the hydrophobicity of their surface. Based on the fact that in both systems the structures of aggregates exhibited the existence of two regions with different fractal dimensions, it was concluded that aggregation was accompanied by restructuring.

Zeiri *et al.*[273] studied a specific process of two-dimensional aggregation, namely, deposition of silver particles, which were distributed over the water subphase/organic liquid interface, on a thin electrode just contacting the water phase. An ensemble of silver particles at the interface (the so-called metallic liquid-like films) was prepared following a special procedure.[274] The organic phases were chloroform and dichloromethane and the water subphases were aqueous solutions of silver nitrate with various surfactant additives. The concentration of silver nitrate in solutions was varied over a wide range. The use of solutions with strongly different concentrations allowed silver deposition on the electrode to be carried out in three regimes, *viz.*, electroaggregation of particles, electrochemical deposition of silver in the absence of interfacial particles and a combined regime 'electro-

aggregation particles/electrochemical deposition of silver'. In the last-mentioned case, aggregation proceeded by a new mechanism, which involved the formation of interparticle bridges due to electrochemical deposition of silver. The preparation of nearly poreless aggregates and wire-like structures revealed the possibility of basically changing the structure of the deposits and their fractal characteristics.

Studies on subtle details of structural organisation of fractal aggregates formed on the liquid surface have been reported [275, 276] taking aggregation of polystyrene latex particles of size 1 μm, which floated in the surface of aqueous solutions, as an example. Analysis of changes in the structure factor $S(q,t)$ under reaction-limited cluster–cluster aggregation conditions [275] revealed a power-law singularity in $S(q,t)$ at $t \to \infty$, $q \to 0$. This behaviour corresponds to the so-called self-organised criticity, where in the absence of external factors the system tends to reach a state characterised by the absence of characteristic time and length scales. The system comprises both small clusters and large clusters whose size is comparable with the size of the entire system. In this case, a crucial role is played by co-operative effects, which reflect the long-range order in the ensemble of two-dimensional aggregates.

Experiments with polystyrene latex particles on liquid substrates were accompanied by numerical simulations of two-dimensional aggregation process at rather high particle concentrations under duffusion-limited cluster–cluster aggregation conditions.[276] Direct observations of the system's structure [numerical processing of the experimentally measured structure factor $S(q,t)$] and the results of numerical simulation showed that at imtermediate times the system has a structure with a six-fold symmetry. The corresponding peaks of the structure factor become strongly diffuse with time. The six-fold symmetry is quite unexpected for the system under study and has no rigorous physical substantiation as yet. It was hypothesised that the instant at which the hexagonal structure is formed corresponds to the instant at which the average cluster size becomes comparable with the half-distance between clusters. At that instant, depletion zones are formed around clusters and weak long-range repulsion between the mobile clusters can provide conditions for the formation of a hexagonal structure. By the way, the authors [276] pointed to weak points of this hypothesis.

Control of the interaction between particles located at the interface was a rather complicated task in most experiments considered above. This fact is responsible for the scatter of the fractal dimension values obtained in different experiments. Hansen and Bergström [277] proposed a method of controlled variation of the potential of interparticle interaction by varying the extent of particle modification by alcohols and the length of the grafted alkyl chain. Estimates revealed that replacement of octyl by an octadecyl chain causes the bond energy of 2 μm silica particles at the air/toluene interface to decrease from 30 down to $15\,kT$. Video-enhanced microscopy and image analysis of the particle dynamics showed that the average cluster size and the cluster size distribution obey the scaling relationship (20). The structure of the octyl system is formed in the diffusion-limited cluster–cluster aggregation regime. This is indicated by the fractal dimension of aggregates determined from the dependence of the radius of gyration on the number of particles and using the grid method ($d_f = 1.45$). Aggregation of particles in the octadecyl system resulted in a more dense structure with $d_f = 1.55$. A feature of both systems is the characteristic time corresponding to a transition point between aggregation regimes, which was attributed to convective motion of the clusters at the interface. Convective motion considerably enhances the mobility of large clusters and is believed to be responsible for the transition from diffusion-limited to reaction-limited cluster–cluster aggregation.

Particles can form gel-like structures both at liquid interfaces and in the bulk of the liquid phase. Two- and three-dimensional gels exhibit no fundamental differences in their behaviour; because of this, we will not consider them. The characteristics of such structures including their rheological properties have been thoroughly studied by Dickinson.[222]

A detailed investigation of two-dimensional aggregation of colloidal particles under the DLA and RLA conditions was reported.[278] Numerical simulation was carried out for the rectangular lattice and off-lattice models. The emphasis was placed on the dependence of the fractal dimension on the initial particle concentration, which varied over a range of two and a half orders of magnitude. The relationship established for the fractal dimension was similar to that obtained for three-dimensional systems

$$d_f = d_{f0} + b_d \varphi^{c_d}.$$

The parameters b_d and c_d in this relationship depend on the aggregation regime and on the model employed. However, the exponent c_d was equal to nearly unity within the limits of the computational procedure. The temporal dependence of the cluster size was also calculated. At a rather long time scale, this is a power law with the exponent z, where z depends on concentration as follows:

$$z = z_0 + b_z \varphi^{c_z}.$$

Here, the values of the coefficients are also governed by the regime of aggregation and the model employed; however, the exponent significantly differs from unity and is close to 0.6.

The subject of the studies considered above was the DLA or RLA regime at the surface of liquid phase. Practical realisation of other mechanisms of aggregation in these systems is a complicated task. The authors of study [279] succeeded in implementing a two-dimensional ballistic aggregation of particles. In the experiments, hydrophobic particles were successively placed at the top of a droplet on the substrate. Particles were gravity 'slipped' following 'linear' trajectories towards the peripheral area of the droplet where aggregation occurred (aggregates grew from the periphery towards the centre of the surface of the spherical segment). The surface was nearly completely covered by particles; the fractal dimension of the aggregates thus grown was 1.95. In the case of diffusion-limited cluster–cluster aggregation on a flat surface, the same particles formed fractal structures with a fractal dimension of 1.45.

Particle aggregation on liquid surfaces in specific regimes (neither DLA nor RLA) is accompanied by the formation of various structures including fractal ones.[280–282]

2. Cluster deposition on substrates

Deposition of nanoparticles on solid substrates is also accompanied by the growth of clusters with fractal structure.[283] Low-energy monodispersed clusters produced by condensation of vapours were vacuum deposited on the substrate, thus forming submonolayers of clusters comprised of several tens to several thousands of atoms. Such clusters do not break down upon collision with the substrate. Larger clusters are characterised by small surface diffusion coefficients; therefore, they virtually do not move across the surface and their aggregation is thus also strongly inhibited. As the number of clusters on the substrate increases, specific structures are formed, which correspond to successive deposition of strongly attaching particles. Most often, structures similar to two-dimensional fractal aggregates are formed. Experimental studies and the results of numerical simulation concerning a broad spectrum of problems related to cluster deposition have been reviewed.[284, 285] However, a study on the growth of fractal germanium clusters by epitaxial deposition on lead-coated silica surface should be pointed out.[286] A remarkable feature of this study is that the cluster structure corresponds to the RLA rather than DLA regime. This indicates the existence of an energy barrier, which precludes aggregation of clusters. The barrier is high enough to provide conditions for transition from the DLA (a common situation for clusters on solid substrates) to RLA regime at small surface diffusion coefficients.

Clusters with fractal structures were produced by pulsed laser deposition of gold vapours on substrate (highly oriented pyrolytic

graphite).[287] The possibility of formation of fractal aggregates in similar experiments with a NaCl substrate was suggested earlier.[288] The fractal dimension depended on the radiation intensity and on the length of the pulse train. An original model for the formation of fractal clusters was proposed. It is based on consideration of the motion of adatoms across the substrate surface. The model was transformed to the equations corresponding to the formation of Julia sets.[111] It correctly reproduced value of the fractal dimension of aggregates.

The subjects of studies [289–294] were various theoretical models for growth of fractal aggregates from particles deposited on solid substrates. The models included the surface diffusion of adatoms [289] and clusters [290] as well as rotation of clusters [291] assuming deposition of both monodisperse particles and particles of different size [292, 293] and shape.[294] Analysis of aggregation on solid substrates also revealed that the fractal dimension is related to the degree of surface coverage as follows

$$d_f = 1.455 + 1.322\,\varphi.$$

Experimental studies in this field [295–299] were concerned with the deposition of metal vapours on the surface of substances with well-developed crystal structure [295, 296] and on the surface of oil [297] and glass.[298] Deposition of mesoscopic particles on a solid substrate was reported.[299]

The fractal structures are formed on the surface not only on deposition of vapours or particles but also in surface chemical reactions. This was observed in the Dy–Co system (see Ref. 300) under the action of a beam in an electron microscope and on the surface of liquid gallium.[301] The formation of iron oxide clusters of size up to several millimetres on the surface of amorphous iron films several tens of nanometres thick was reported.[302] In all experiments, the cluster structures were identical to the structure of the particles grown in the DLA regime. The results of recent search for fractal structures on the surfaces of specially treated polymer films are available.[303, 304]

VII. Viscous fingering

Penetration of fluids into porous solids also produces fractal structures.[13] Fluid flow in porous media is accompanied by the so-called viscous fingering, *i.e.*, formation of a specific kind of prominence at the interface. Viscous fingering is due to the instability of the propagating interface and usually occurs when the more viscous fluid is displaced from the porous media by the less viscous fluid. The fractal dimension of viscous fingers is determined using the following relationship

$$N_v = k_v R_g^{d_f}, \tag{52}$$

where N_v is the number of pores filled with the more viscous fluid, k_v is the corresponding prefactor and R_g is the radius of gyration of the liquid cluster. Studies on the mechanisms of viscous fingering and formation of related structures have been well documented.[305, 306]

Viscous fingering is most often analysed taking immiscible fluids [13] and — much more rarely — partially miscible fluids [307] as examples. This phenomenon can also occur when dispersions are displaced by neat solvents, because the former liquids are always more viscous than the latter.

The so-called Hele–Shaw flow, or displacement of a viscous fluid from the space confined between two transparent flat plates, is often considered as a model for flow in a porous medium. Transparency of the plates allows the propagation of the interface to be monitored.[308] A complete analogy between the development of instabilities of the Hele–Shaw flow and the growth of dendritic structures was established.[306, 309] Stability studies of the Hele–Shaw flow are of great practical value, because the development of instabilities precludes a number of important technological processes related to, *e.g.*, oil displacement from pools. For this reason, attempts to suppress the development of instabilities are undertaken. Studies on the flow of three immiscible fluids in the Hele–Shaw cell [310] and on the flow stability considerations in the presence of highly dispersed particles in the displacing fluid [311] showed that under particular conditions it is possible to suppress the development of instabilities in different stages of flow.

There is an analogy between the flow in porous solids and fractal aggregation. In particular, the DLA model and the flow in porous solids are described by identical equations.[13, 312, 313] However, this analogy does not necessarily hold. The laws of formation of the viscous interface in the case of porous solids characterised by a broad pore size distribution are significantly different from the laws of clustering under the DLA conditions.[314]

The influence of inhomogeneities in the porous medium on the regularities of the growth of viscous fingers has been studied assuming a Gaussian distribution of the permeability of the porous medium centred at the mean value.[315] The fractal structure of viscous fingers was not determined. The authors calculated the width of the mixing interface between two fluids for different dispersions of the permeability (see also Section VIII). According to calculations, the width of the interface increases linearly with time.

Viscous fingering related to flow in fractal structures was studied.[316] This is the case of flow in, *e.g.*, porous media near the percolation threshold (at a small fraction of through pores). Clearly, in this case the fractal system of viscous fingers will also be governed by the structure of the percolation cluster of the porous solid. More sophisticated models for viscous fingering in porous media require the use of the multifractal approach to describe the media [317] or the self-affine geometry for the pore space.[318]

Viscous fingering accompanied by polymerisation at the interface was simulated.[319] It was shown that three situations are possible depending on the capillary number

$$N_{Ca} = \frac{\eta \upsilon}{\gamma},$$

where η is the viscosity of the displacing fluid, υ is the average interface propagation velocity and γ is the interfacial tension. Within some range, the reaction rate affects the interface propagation velocity; at lower reaction rates beyond the range mentioned above, the reaction has virtually no effect on the interface propagation. At higher rates (above the upper bound of the range), the interface propagation slows down. The smaller the capillary number, the wider the range of reaction rates affecting interface propagation.

The theoretical studies considered above were carried out using mainly two-dimensional models of porous media. Numerical solution to the three-dimensional hydrodynamics equations describing viscous fingering in the case of partially miscible fluids was also reported.[320] It was shown that screening, spillover and coalescence of viscous fingers occur at all Peclet numbers in the range studied. At large Peclet numbers, splitting of viscous fingers occurs, similarly to two-dimensional systems. Broadening of the interface at long time scales occurs at a constant velocity, which is independent of the Peclet number. If flow occurs in the regime corresponding to rare splitting of viscous fingers, their number monotonically decreases with time. The authors pointed out that the solution obtained for the two-dimensional model by and large correctly includes peculiar features of the development of the process in three-dimensional systems.

A related study [321] dealt with the effect of kinetic fluctuations on the propagation of the interface between immiscible fluids. According to calculations, the width of the interface remains constant for three-dimensional systems. For the two-dimensional model of a porous medium, the interface width logarithmically increases with time.

A more complex process, namely, displacement of a viscous fluid from the porous body by the medium that can react with the body (dissolve it) was also studied.[322, 323] It was found that the

structure of the liquid – liquid interface is similar to the interface structure formed in the DLA regime. The results of simulation of the structure of a soluble porous solid were confirmed experimentally. This problem was also solved analytically [324] in the asymptotic limit using the renormalisation group method. This system is characterised by the existence of two limiting regimes. Under these conditions, the interface structure corresponds to the structure of the DLA-grown clusters and it is possible to observe a successive transition from the interface with the structure of the DLA-grown clusters to a rather smooth interface and then again to the interface with the structure of the DLA-grown cluster.

Studies of the boundary effects on the structure of viscous fingers [68] revealed that the fractal dimension of viscous fingers in retarded flow is much smaller than in the three-dimensional system. As the bounding surfaces move away, the fractal dimension logarithmically approaches its bulk value.

Fractal structures are also formed when nonwetting fluids displace wetting fluids from porous solids. In particular, this is the case for the conventional mercury porosimetry technique.[325] Simulation is usually carried out using a particular (prescribed) structure of pores and pore necks, which permits the fractal dimension of the growing structures to be varied over a rather wide range. Usually, the entire percolation cluster of the invaded fluid, its branches and the 'backbone', which is obtained by cutting the branches off, are considered.[326–330] The structure of the porous solid has a strong effect not only on the fractal characteristics of different clusters but also on their structure.[329] This holds for the systems both with and without trapping of the displaced fluid.

Viscous fingering was observed during the wetting/dewetting process of a solid surface.[331] In the experiments, a droplet of SnPb eutectic alloy at first spilled over an Au/Cu/Cr multilayered film. This droplet etched the Au/Cu films, which was followed by contraction of the droplet, because the chromium substrate was not wetted with the alloy. It was found that contraction of the droplet was accompanied by the formation of fractal structures similar to viscous fingers. At different stages of contraction, fractal structures with different structures were formed. At first, the fractal structure exhibited a DLA pattern, while the final structure was a dendrite-like one. The fractal dimensions of these structures were 1.83 and 1.79, respectively.

The problem of the flow of a fluid along the grain boundaries [332] is similar to the viscous fingering problem. The grain boundaries wetted with the fluid form a fractal cluster, which allows percolation transitions to be observed similarly to the case of fluid invasion into porous media.

VIII. Fractal films

1. Simulation

Recently, considerable attention has been given to the studies of vapour deposition of films.[333] This is due to two reasons. On the one hand, vapour-deposited metal and semiconductor films are used in various microelectronic devices. On the other hand, development of scanning electron and atomic force microscopies has opened up new prospects for research on the properties of films and on the mechanisms of their growth.

Vapour phase deposition of films is usually accompanied by the formation of granular structures (protrusions of different height and width). Here, significant roles are played by the thermodynamics and kinetics of film growth. Thermodynamics predetermines the growth pattern (layer-by-layer or island-type) of the newly formed structure, while the kinetics prescribes the rates of nucleation and growth of islands (*via* parameters of the surface diffusion of atoms). The formation of a continuous surface layer is followed by the growth of films with rough surface, the roughness being more pronounced with time. This is due to the fact that protrusions 'mask' depressions, thus making them less accessible to filling. This mechanism of development of rough surfaces is realised in combination with the smoothing mechanisms of film surfaces, among which the most important is surface diffusion.

Growth of vapour-deposited films is usually described using the ballistic model,[334] according to which particles moving towards the surface follow random trajectories. The surfaces growing by this mechanism possess fractal properties. As mentioned above, fractals can be self-similar or self-affine. Rough surfaces are treated as self-affine objects.

The fractal dimensions of the growing films are usually determined from the dependence of the surface 'thickness' on the lateral size of the portion L rather than the fractal dimension of the profile. The surface thickness is calculated as the root-mean-square deviation of the profile over the length L

$$w(L) = \sqrt{\frac{1}{N_L}\sum_{j=1}^{N_L}\left[h_{fj} - \langle h_f(L)\rangle\right]^2}\,, \tag{53}$$

where N_L is the number of points of the profile of length L, h_{fj} is the height at the point j, and $\langle h_f(L)\rangle$ is the average height of profile of length L. Since the height h_f is a function of time, the surface thickness $w(L,t)$ also appears to be time dependent. For self-affine surfaces, $w(L,t)$ changes with increasing L as follows

$$w(L,t) \propto L^{\alpha},$$

where α is the roughness exponent. For fractal surfaces, the roughness exponent is related to the fractal dimension

$$d_f = d' + 1 - \alpha,$$

where d' is the dimension of the interface (for non-fractal surfaces, $d' = 2$).

Using the ballistic model [335] and Eden model [336] for particle deposition on the substrate, it was established that the surface thickness is described by a universal (scaling) distribution

$$w(h_f) \sim L^{\alpha} f\left(\frac{h_f}{L^{\alpha/\beta}}\right), \tag{54}$$

where h is the average height of the layer deposited on the substrate, L is the width of the growing stripe (column in the case of three dimensions) and the function $f(x)$ meets the following conditions

$$f(x) = \begin{cases} x^{\beta}, & x \ll 1 \\ \text{const}, & x \gg 1 \end{cases}. \tag{55}$$

The parameters in relationship (54) are as follows: $\alpha = 1/2$ and $\beta = 1/3$ for two-dimensional systems and $\alpha = 1/3$ and $\beta = 1/4$ for three-dimensional systems. In the case of the ballistic mechanism, the deposit is a homogeneous medium while the layer deposited has a self-affine 'surface' with fractal structure.

Relationships (54) and (55) were verified for various models [337] including those for 'tree-like' film growth (Fig. 14). Some additional scaling relationships for the tree height, h_f, tree width, w, and for the number, N_s, of trees of size s (s is the number of particles in the tree) were established. They are as follows

$$w \sim s^{\nu_1}, \tag{56}$$
$$h_f \sim s^{\nu_2},$$
$$N_s \sim s^{-\tau},$$

where the exponents are interrelated

$$(d-1)\nu_1 + \nu_2 = 1, \tag{57}$$
$$\tau = 2 - \nu_2,$$

and weakly depend on the deposition model employed.

When analysing the dynamics of film growth, relationship (54) can be re-written in the more general form

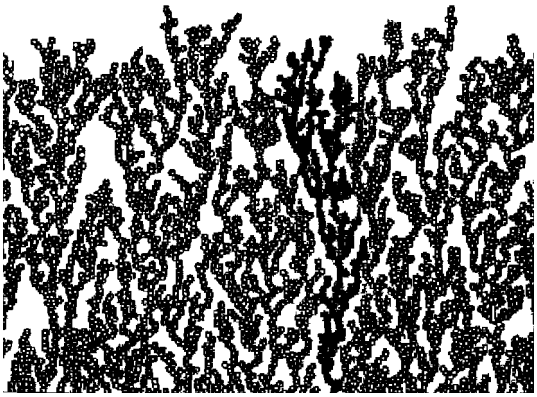


Figure 14. Structure of fractal aggregates formed upon deposition of particles on substrates.
As can be seen, the number of 'trees' grown on the surface sequentially decreases (one 'tree' is shown in black).

$$w(t) \sim l^{\alpha} f\left(\frac{t}{L^{\alpha/\beta}}\right), \tag{58}$$

where t is time.

Various equations were proposed for analytical description of the film growth during vapour and particle deposition on the substrate. Consider the most important of them.

The simplest model was proposed by Edwards and Wilkinson.[338] Here, the height of the surface is determined from the equation

$$\frac{\mathrm{d}h_{\mathrm{f}}}{\mathrm{d}t} = v\nabla^2 h_{\mathrm{f}} + \chi(x,t), \tag{59}$$

where $\chi(x,t)$ denotes the fluctuation (noise) contribution of the surface; $\chi(x,t)$ meets the following conditions

$$\langle \chi(x,t) \rangle = 0, \tag{60}$$

$$\langle \chi(x,t)\chi(x',t') \rangle = R\delta(x-x')\delta(t-t'),$$

where the angle brackets denote the averaging over the random variable χ, R is root-mean-square fluctuation of 'noise'.

This model describes smoothing of the surface by the capillary forces governed by the parameter v. The model can also be used to describe the propagation of an interface through a disordered medium and to study how the interface spreads out with time.[339]

The parameters of the model are as follows: $\alpha = (3-d)/2$ and $\beta = (3-d)/4$ for a one-dimensional substrate and $\alpha = 1/2$ and $\beta = 1/4$ for a two-dimensional substrate; the width of the surface logarithmically increases with time; for substrates of greater dimensions, the surface of the growing film is considered smooth.

This model was employed[340] in calculations of interface growth on a fractal substrate characterised by the dimension d_{s}. The surface width exhibits the asymptotic behaviour given by expressions (54) and (55) with the parameter β

$$\beta = \begin{cases} \dfrac{1}{4}, & d' = 1 \\ \dfrac{1}{4} - \dfrac{d_{\mathrm{s}}}{4}, & 1 < d_{\mathrm{s}} < 2, \end{cases} \tag{61}$$

where d' is the substrate dimension.

A similar expression was obtained for the parameter α[341]

$$\alpha = \begin{cases} \dfrac{1}{2}, & d' = 1 \\ d_{\mathrm{f}}\left(\dfrac{1}{d_{\mathrm{s}}} - \dfrac{1}{2}\right), & 1 < d_{\mathrm{s}} < 2. \end{cases} \tag{62}$$

The Edwards–Wilkinson model correctly reproduces the structure of surfaces grown by sedimentation of spherical particles.[342] Experiments were carried out with particles of size 440 nm in aqueous solutions. The profile of the sediment surface was determined using an atomic force microscope.

Trapping of polystyrene latex particles of size 0.8 μm at the meniscus of a thin film was studied in experiments on a deposition on a 'one-dimensional' substrate.[343] It was found that $\beta = 0.267$, while the parameter α varied from 0.5 in the initial stage of the 'surface' growth to 0.71 a long time after the beginning of the process. The crossover of the regimes of the surface growth was explained by kinetic reasons. Initially, the 'deposit' moves with the meniscus and particles are deposited ballistically. Then, the deposit slows down and deposition due to Brownian-type particle diffusion is observed.

Kardar, Parisi and Zhang[344] proposed a more sophisticated model for film growth, which is described by the following equation

$$\frac{\mathrm{d}h_{\mathrm{f}}}{\mathrm{d}t} = v\nabla^2 h_{\mathrm{f}} + \frac{\lambda}{2}(\nabla h_{\mathrm{f}})^2 + \chi(x,t), \tag{63}$$

here λ is the parameter of a model.

The additional term [*cf.* Eqn (59)] accounts for smoothing of the surface by lateral growth of protrusions. In the case of two dimensions, this model gives the parameters $\alpha = 1/2$ and $\beta = 1/3$, which exactly fulfils the relationship predicted[345] for Eqn (63)

$$\alpha + \frac{\alpha}{\beta} = 2.$$

A comprehensive examination of Eqn (63) was reported.[346, 347] The parameters of Eqn (63) were related to the coefficients determining the asymptotic behaviour of the surface width at long time and long length scales

$$w(\infty, t) = C_t t^{1/3}, \tag{64}$$

$$w(L,\infty) = C_L L^{1/2},$$

The possibility of deriving a single-parameter (λ) universal relationship for the coefficients C_t, C_L was shown. Analogous analysis of the model for epitaxial film growth[348] is described by the following equation

$$\frac{\mathrm{d}h_{\mathrm{f}}}{\mathrm{d}t} = -v\nabla^4 h_{\mathrm{f}} + \lambda\nabla^2(|\nabla h_{\mathrm{f}}|)^2 + \chi(x,t); \tag{65}$$

the model gives the parameters $\alpha = (5-d)/3$ and $\beta = (7+d)/3$ and is consistent with the results of numerical simulation of film deposition at the atomic level.

Various analytical models for film growth and interface propagation were proposed[349–355] to generalise the models considered above. The model by Kardar–Parisi–Zhang was extended[356] to the case for radial growth of spherical surfaces. The surface width is a complex function of time and exhibits a power dependence on a rather long time scale, the parameter β being equal to 1/3. Numerical simulation of the co-deposition of films was carried out[357] with inclusion of the interactions between nearest neighbours and more distant particles and different probabilities of the deposition of the particles of a specified type at a given instant. It was shown that the parameters α and β depend on this probability, thus exhibiting a marked deviation from the dependence predicted by Eqn (63).

New models for particle deposition on substrates resulting in the formation of fractal surfaces have also been developed. In particular, an original model was proposed,[358] which accounts for hierarchical deposition of debris during particle deposition from the atmosphere (particles reach the surface in order of size, largest first). Both regular and stochastic models for particle deposition on substrates were considered. Numerical simulation revealed that, in contrast to deposition of particles of the same size, in this

model the contour length (or surface area) increase logarithmically rather than obeying the power law as the length scale changes. For instance, the length of a line on the surface increases on decreasing the characteristic probe size δ as follows:

$$L(\delta) = \left(1 + A \ln \frac{1}{\delta}\right) L(1),$$

where A is a constant.

2. Experiments

Experimental studies on the interface growth were carried out using various systems.[351] The physical meaning of the equations considered above corresponds to the molecular beam epitaxy experiments. Deposition of gold,[359–362] silver [359,363] and iron [359,364–366] films on various substrates was studied. A rather wide scatter of α values was obtained, which is apparently due to the use of different methods of determination of surface roughness. However, the scatter of β values is much smaller compared to that of α values. At the same time, in most cases the results of calculations and experimental data are in good agreement. This can be exemplified by the results of a study [367] concerned with the analysis of the evolution of the surface of gold films deposited using the thermal evaporation technique. The characteristics of the surface were determined using scanning tunnelling microscopy; the experimental data were processed using Fourier analysis, which allowed the so-called power spectrum, $S_m(q,t)$, of the protrusion heights to be calculated. It was found that the surface width depends on time as $t^{0.25}$ and the power spectrum

$$S_m \sim q^{-4.1},$$

the parameter α being equal to nearly unity.

The dynamics of the interface growth was studied not only in the film deposition experiments but also in the experiments on paper imbibition,[368–370] combustion [371] and tear.[372] The experimental results were described by the power dependences (54)–(58) but the values of the exponents differed from those predicted by theoretical models; the numerical values of the exponents obtained in different experiments were also different (for instance, paper imbibition experiments gave close values of the parameters α and β). Yet another feature of the experimental data is the crossover of the growth regimes of the interface width, which manifested itself as a change in the exponents α and β on increasing the time and length scales. No unambiguous explanation for this phenomenon has been reported as yet. It should be noted that some theoretical models include the possibility of changing the interface growth regime (see, *e.g.*, Ref. 350). This change can be due to large-scale fluctuations of the growth direction in the active zone. However, the available models for growth of self-affine surfaces cannot correctly describe this crossover.[350] Numerical experiments [373] on epitaxial growth of the surface with inclusion of surface diffusion without desorption of adatoms revealed two growth regimes of the interface width. The regime found for short time scales was changed to that described by the Kardar–Parisi–Zhang equation over a long time scale. The new growth regime at short times is due to the inclusion of surface diffusion and is not observed if diffusion processes are ignored.

The establishment of different growth regimes is a complicated task because modification of models does not necessarily lead to crossover. In this connection, a representative example is provided by the study [374] on a modified Eden model in which the growth process began after contact with 'acceleration sites', which were spatially distributed at random. The 'acceleration site' became an Eden cell immediately after contact with the surface of the growing film. The model revealed a percolation transition, *i.e.*, the existence of some critical concentration of 'acceleration sites' corresponding to divergence of the growth rate of the surface area. However, no crossover of the growth regimes was found, even for this, basically modified, model. Moreover, the value of the exponent α remained constant (0.5) over a wide range of 'acceleration site' concentrations.

The problem of etching of metallic surfaces is closely related to the problems considered above. It was reported [375] that the perimeters of pits etched in thin aluminium films in NaCl solutions have a fractal structure and that the 'roughness' of the perimeter developed only at particular values of the potential applied. Detailed analysis of the corrosion pit profiles (corroded surface of stainless steel rods) [376] revealed two different length scales (textural and structural) with different fractal dimensions (1.17 and 1.45, respectively). Further studies confirmed the existence of two characteristic length scales for the corrosion pit profiles in steel rods and aluminium sheets. Two fractal dimensions were also reported [377] in a study of corrosion of vapour-deposited nanoscale Al films; the larger fractal dimension corresponded to the longer length scale. It was shown that the pit morphology can be varied over a rather wide range by varying the concentrations of iron and chloride ions in solution.[377] Transition from a smooth to rough interface under particular regimes of corrosion is also possible.[378] Corrosion of quasi-two-dimensional thin Al films was studied.[379] Both model and numerical experiments were carried out. Model experiments were carried out using Al films 50 μm thick with etched end faces. Numerical simulation was performed with inclusion of higher electrolyte concentration in the pit during corrosion. The pit perimeter was characterised by one fractal dimension, which to some extent varied depending on the procedure employed for its determination. The results of the model and numerical experiments were found to be in good agreement.

Numerical (Monte Carlo) simulation of dissolution of a solid was carried out [380] taking the case for the dissolution rate controlled by surface reactions as an example. It was shown that the predominance of stochastic lateral dissolution causes broadening of the interface; the parameters of Eqn (58) were found to be $\alpha = 1/3$ and $\beta = 1/4$. The inclusion of surface diffusion of atoms led to an increase in the α value to unity (β value remained unchanged) in the early stages and to transition to unstable interface in the later stages (β value increased from 0.25 to greater than 0.5). The inclusion of nonlocal effects caused an even greater increase in the parameter β.

* * *

In this review we considered the most important characteristics of fractal objects and the main types of fractal structures which can be found in disperse systems. The material presented gives an idea of the diversity of fractal objects and parameters that are necessary to completely characterise them. The large number of parameters reflects the variety of specific properties of fractal structures, which do or do not manifest themselves depending on external conditions. An attempt to present a comprehensive analysis of the properties of even those fractal structures considered in this review could lead to a considerable increase in the size of the text. Because of this, experimental methods for the determination of the fractal characteristics and physicochemical properties of fractal objects will be described separately.

References

1. B B Mandelbrot *Fractals: Form, Chance, and Dimension* (San Francisco: Freeman, 1977)
2. B B Mandelbrot *The Fractal Geometry of Nature* (San Francisco: Freeman, 1982)
3. B M Smirnov *Usp. Fiz. Nauk* **149** 177 (1986) [a]
4. B M Smirnov *Usp. Fiz. Nauk* **152** 133 (1987) [a]
5. I M Sokolov *Usp. Fiz. Nauk* **150** 221 (1986) [a]
6. H J Herrman *Phys. Rep.* **136** 153 (1986)
7. P Meakin *Ann. Rev. Phys. Chem.* **39** 237 (1988)
8. R Zhyul'en *Usp. Fiz. Nauk* **157** 339 (1989) [a]
9. A I Olemskoi, F Ya Flat *Usp. Fiz. Nauk* **163** 1 (1993) [a]

10. E P Emets, A E Novoselova, P P Poluektov *Usp. Fiz. Nauk* **164** 959 (1994); [*Physics Uspekhi* **37** 881 (1994)]
11. E F Mikhailov, S S Vlasenko *Usp. Fiz. Nauk* **165** 263 (1995); [*Physics Uspekhi* **38** 253 (1995)]
12. B M Smirnov *Fizika Fraktal'nykh Klasterov* (The Physics of Fractal Clusters) (Moscow: Nauka, 1991)
13. J Feder *Fractals* (New York: Plenum, 1988)
14. V V Zosimov, L M Lyamshev *Usp. Fiz. Nauk* **165** 361 (1995) [*Physics-Uspekhi* **38** 347 (1995)]
15. V M Shalaev *Phys. Rep.* **272** 61 (1996)
16. T Vicsek *Fractal Growth Phenomena* (Singapore: World Scientific, 1992)
17. A K Sarychev, V M Shalaev *Phys. Rep.* **335** 276 (2000)
18. P Meakin *Fractals, Scaling and Growth Far from Equilibrium* (Cambridge; Cambridge University Press, 1998)
19. P Meakin *J. Sol-Gel Sci. Technol.* **15** 97 (1999)
20. V V Vysotskii, V I Roldughin *Kolloid. Zh.* **60** 729 (1998) [b]
21. V I Roldughin, V V Vysotskii *Prog. Org. Coat.* **39** 81 (2000)
22. V U Novikov, G V Kozlov *Usp. Khim.* **69** 378 (2000) [*Russ. Chem. Rev.* **69** 347 (2000)]
23. V U Novikov, G V Kozlov *Usp. Khim.* **69** 572 (2000) [*Russ. Chem. Rev.* **69** 523 (2000)]
24. S R Forrest, T A Witten *J. Phys. A: Math. Gen.* **12** L109 (1979)
25. T A Witten, L M Sander *Phys. Rev. Lett.* **47** 1400 (1981)
26. P Meakin *Phys. Rev. Lett.* **51** 1119 (1983)
27. M Kolb, R Botet, R Jullien *Phys. Rev. Lett.* **51** 1123 (1983)
28. D A Weitz, M Oliveria *Phys. Rev. Lett.* **52** 1433 (1984)
29. D A Weitz, J S Huang, M Y Lin J Sung *Phys. Rev. Lett.* **54** 1416 (1985)
30. D A Weitz, M Lin, C Sandroff *Surf. Sci.* **158** 147 (1985)
31. M Matsushita, M Sano, Y Hayakawa, H Honjo, Y Samada *Phys. Rev. Lett.* **53** 286 (1984)
32. R M Brady, R C Ball *Nature (London)* **309** 225 (1984)
33. J Nittmann, J Daccord, H Stanley *Nature (London)* **314** 141 (1985)
34. P Dimon, S K Sinha, D A Weitz, C R Safinya, G S Smith, W A Varady, H M Lindsay *Phys. Rev. Lett.* **57** 595 (1986)
35. D Avnir, D Farin, P Pfifer *J. Chem. Phys.* **79** 3566 (1983)
36. H D Bale, P W Schmidt *Phys. Rev. Lett.* **53** 596 (1984)
37. D Avnir, D Farin, P Pfifer *Nature (London)* **308** 261 (1984)
38. R Amal, J A Paper, T D Waite *J. Colloid Interface Sci.* **140** 158 (1990)
39. G C Bushell, R Amal, J A Paper *Physica A* **233** 859 (1996)
40. J E Martin, J P Wilcoxon, D Schaefer, J Odinek *Phys. Rev. A* **41** 4379 (1990)
41. Z Zhou, B Chu *J. Colloid Interface Sci.* **143** 356 (1991)
42. C M Sorensen, J Cai, N Lu *Appl. Opt.* **31** 6547 (1992)
43. L Pietronero, E Tosatti (Eds) *Fractals in Physics* (Amsterdam: North-Holland, 1986)
44. P Meakin *Phys. Rev. A* **33** 1365 (1986)
45. P Grassberger *J. Phys. (Paris)* **46** 1543 (1985)
46. P Meakin, H E Stanley, A Coniglio, T A Witten *Phys. Rev. A* **32** 2364 (1985)
47. P Meakin, A Coniglio, H E Stanley, T A Witten *Phys. Rev. A* **34** 3325 (1986)
48. T C Halsey, P Meakin *Phys. Rev. A* **32** 2546 (1985)
49. C M Sorensen, N Lu, J Cai *J. Colloid Interface Sci.* **174** 456 (1995)
50. S K Sinha, T Freltoft, J Kjems, in *Kinetics of Aggregation and Gelation* (Eds F Family, P Landau) (Amsterdam: Elsevier, 1984)
51. R D Mountain, G W Mulholland *Langmuir* **4** 1321 (1988)
52. R Jullien *J. Phys. I (France)* **2** 759 (1992)
53. M V Lin, R Klein, H M Lindsay, D A Weitz, R C Ball, P Meakin *J. Colloid Interface Sci.* **137** 263 (1990)
54. P J Mors, R Botet, R Jullien *J. Phys. A: Math. Gen.* **20** L975 (1987)
55. R Jullien, R Botet, P M Mors *Discuss. Faraday Soc.* **83** 125 (1987)
56. S Kim, J R Brock *J. Appl. Phys.* **60** 509 (1986)
57. S Kim, J R Brock *J. Colloid Interface Sci.* **116** 431 (1987)
58. P Meakin *J. Colloid Interface Sci.* **134** 235 (1990)
59. P Meakin, M Muthukumar *J. Chem. Phys.* **91** 3212 (1989)
60. P Meakin, R Jullien *J. Chem. Phys.* **89** 246 (1988)
61. R Jullien, P Meakin *J. Colloid Interface Sci.* **127** 265 (1989)
62. P Meakin, S Miyazima *J. Phys. Soc. Jpn.* **57** 4439 (1988)
63. S Ohta, H Honjo *Phys. Rev. A* **44** 8425 (1991)
64. V Tchijov, S Nechaev, S Rodriguez-Romo *Pis'ma ZhETF* **64** 504 (1996) [c]
65. J-M Debierre, G Albient *J. Phys. A: Math. Gen.* **29** 1905 (1996)
66. N Vandewalle, M Ausloos *Phys. Rev. E* **50** R635 (1994)
67. A M Zatevalov, V I Roldughin, I A Tutorskii *Kolloid. Zh.* **62** 483 (2000) [b]
68. R Cafiero, G Caldarelli, A Gabrielli *Phys. Rev. E* **56** R1291 (1997)
69. N I Lebovka, N V Vygornitskii, V V Mank *Kolloid. Zh.* **59** 336 (1997) [b]
70. J F Dirkse, J D Cawley *J. Colloid Interface Sci.* **170** 466 (1995)
71. F Porcu, F Prodi *Phys. Rev. A* **44** 8313 (1991)
72. T L Farias, Ü Ö Köylü, M G Carvalho *J. Quant. Spectrosc. Radiat. Transfer.* **55** 357 (1996)
73. M Tence, J P Chevalier, R Jullien *J. Phys. (Paris)* **47** 1989 (1986)
74. A Hasmy, M Foret, J Pelous, R Jullien *Phys. Rev. B* **48** 9345 (1993)
75. A Hasmy, R Vacher, J Pelous, R Jullien *Phys. Rev. B* **50** 1305 (1994)
76. G Bushell, R Amal *J. Colloid Interface Sci.* **205** 459 (1998)
77. H Kesten *J. Phys. A: Math. Gen.* **20** L29 (1987)
78. M Tokuyama, K Kawasaki *Phys. Lett. A* **100** 337 (1984)
79. H G E Hentschel *Phys. Rev. Lett.* **52** 212 (1984)
80. P.-G. de Gennes *Scaling Concepts in Polymers Physics* (Itaca, NY: Cornell University Press, 1979)
81. H Gould, F Family, H E Stanley *Phys. Rev. Lett.* **50** 686 (1983)
82. J L Montag, F Family, T Wicsek *Phys. Rev. A* **32** 2557 (1985)
83. S Ma *Modern Theory of Critical Phenomena* (London: Benjamin, 1976)
84. L M Sander, P Ramanlai, E Ben-Jakob *Phys. Rev. A* **32** 3160 (1985)
85. E Louis, O Pal, L M Sander, F Guinea *Mod. Phys. Lett. B* **8** 1739 (1994)
86. E Ben-Jakob, P Garik *Nature (London)* **343** 523 (1990)
87. D G Grier, D Mueth *Phys. Rev. E* **48** 3841 (1993)
88. E Brener, H Müller-Krumbhaar Y Saito, D Temkin *Phys. Rev. E* **47** 1151 (1993)
89. L M Martyushev, V D Seleznev, S A Skopinov *Pis'ma ZhTF* **23** 1 (1997) [d]
90. M M Khvorov, T M Shvets *Kolloid. Zh.* **53** 564 (1991)
91. J K Lin, D G Grier *Phys. Rev. E* **54** 2690 (1996)
92. L M Martyushev, V D Seleznev, S A Skopinov *Kristallografiya* **42** 753 (1997) [e]
93. L M Martiouchev, V D Selesnev, S A Skopinov *J. Stat. Phys.* **90** 1413 (1998)
94. P K Galenko, M D Krivilov, S V Buzinov *Phys. Rev. E* **55** 611 (1997)
95. C S Strom, X-Y Liu, M Wang *J. Phys. Chem. B* **104** 9638 (2000)
96. H Honjo, S Ohta, M Matsushita *J. Phys. Soc. Jpn.* **55** 2487 (1986)
97. E Brener, H Müller-Krumbhaar, D Temkin, T Abel *Physica A* **249** 73 (1998)
98. H Gao, Z Xue, Q Wu, S Pang *Solid State Commun.* **97** 579 (1996)
99. I M Sandler, G F Canright, H Gao, S Pang, Z Xue, Z Zhang *Phys. Rev. E* **58** 6015 (1998)
100. K Honda, H Toyoki, M Matsushita *J. Phys. Soc. Jpn.* **55** 707 (1986)
101. M Matsushita, K Honda, H Toyoki, Y Hayakawa, H Kondo *J. Phys. Soc. Jpn.* **55** 2618 (1986)
102. Y Hayakawa, H Kondo, M Matsushita *J. Phys. Soc. Jpn.* **55** 2479 (1986)
103. K Ohno, K Kikuchi, H Yasuhara *Phys. Rev. A* **46** 3400 (1992)
104. V I Roldughin, D V Voronin *Kolloid. Zh.* **63** 394 (2001) [b]
105. D A Tomalia, A M Naylor, W A Goddart III *Angew. Chem., Int. Ed. Engl.* **29** 138 (1990)
106. J M J Frechet, C J Hawker, K I Wooley *JMS-Pure Appl. Chem. A* **31** 1627 (1994)
107. A M Muzafarov, E A Rebrov *Vysokomol. Soedin., Ser. C* **42** 2015 (2000) [f]
108. P G deGennes, H Hervet *J. Phys. (Paris)* **44** L351 (1983)
109. P Ossadnik *Phys. Rev. A* **45** 1058 (1992)
110. B McCoy *J. Colloid Interface Sci.* **216** 235 (1999)

111. M Shröder *Fractals, Chaos, Power Laws* (New York: Freeman, 1990)
112. A Bershadskii *Chaos, Solitons Fractals* **13** 185 (2002)
113. L Gmachowski *Chem.-Ing.-Tech.* **73** 87 (2001)
114. L M Martyushev, V D Seleznev, I E Kuznetsova *Zh. Eksp. Teor. Fiz.* **118** 149 (2000) [g]
115. A Fernandez-Barbero, A Schmitt, M Cabrerizo-Vilchez, R Martinez-Garcia *Physica A* **230** 53 (1996)
116. D W Mackowski *Appl. Opt.* **34** 3535 (1995)
117. R Thoury, R Jullien *J. Phys. A: Math. Gen.* **27** 2953 (1994)
118. A M Brasil, T L Farias, M G Carvalho *J. Aerosol Sci.* **30** 1379 (1999)
119. A V Filippov, M Zurita, D E Rosner *J. Colloid Interface Sci.* **229** 261 (2000)
120. J Cai, N Lu, C M Sorensen *J. Colloid Interface Sci.* **171** 470 (1995)
121. M K Wu, S K Friedlander *J. Colloid Interface Sci.* **159** 246 (1993)
122. Ü Ö Köylü, G M Faeth, T L Farias, M G Carvalho *Combust. Flame* **100** 621 (1995)
123. S N Rogak, R Flagan *Aerosol Sci. Technol.* **18** 25 (1993)
124. C M Sorensen, G D Feke *Aerosol Sci. Technol.* **25** 328 (1996)
125. C M Sorensen, G Roberts *J. Colloid Interface Sci.* **186** 447 (1997)
126. Ü Ö Köylü, G M Faeth *J. Heat Transfer* 116 152 (1994)
127. Ü Ö Köylü, Y Xing, D E Rosner *Langmuir* **11** 4848 (1995)
128. R Sempere, D Bourett, T Woignier, J Phalippou, R Jullien *Phys. Rev. Lett.* **71** 3307 (1993)
129. A P Weber, U Baltensperge, H W Gaggeler, A Schmidt-Ott *J. Aerosol Sci.* **27** 915 (1996)
130. C Oh, C M Sorensen *J. Colloid Interface Sci.* **193** 17 (1997)
131. M Tirado-Miranda, A Schmitt, J Callejas-Fernandez, A Fernandez-Barbero *Langmuir* **16** 7541 (2000)
132. T Vicsek, F Family *Phys. Rev. Lett.*, **52** 1669 (1984)
133. M H Ernst, in *Non-Equilibrium Phenomena I. The Boltzman Equation, Studies in Statistical Mechanics* (Eds E W Montroll, J L Lebowitz) (Amsterdam: North-Holland, 1983)
134. G van Dongen, M H Ernst *Phys. Rev. Lett.* **54** 1396 (1985)
135. F Ferri, M Giglio, E Paganini, U Perini *Europhys. Lett.* **7** 599 (1988)
136. S N Rogak, R C Flagan *J. Colloid Interface Sci.* **151** 203 (1992)
137. M M R Williams *Ann. Nucl. Energy* **17** 161 (1990)
138. S Vemury, S E Pratsinis *J. Aerosol Sci.* **26** 175 (1995)
139. S H Park, R Xiang, K W Lee *J. Colloid Interface Sci.* **231** 129 (2000)
140. K E J Lehtinen, M R Zachariah *J. Collod Interface Sci.* **242** 314 (2001)
141. K Wu, S K Friedlander *J. Aerosol Sci.* **24** 273 (1993)
142. P J Dekkers, S K Friedlander *J. Colloid Interface Sci.* **248** 295 (2002)
143. P J Dekkers, I L Tuinman, J C M Marijnissen, S K Friedlander, B Scarlett *J. Colloid Interface Sci.* **248** 306 (2002)
144. S H Park, K W Lee *J. Colloid Interface Sci.* **233** 117 (2001)
145. K E J Lehtinen, R S Windeler, S K Friedlander *J. Aerosol Sci.* **27** 883 (1996)
146. P Tandon, D E Rosner *J. Colloid Interface Sci.* **213** 273 (1999)
147. D L Wright, R McGrow, D E Rosner *J. Colloid Interface Sci.* **236** 242 (2001)
148. K H Gardner, T L Theis *J. Colloid Interface Sci.* **180** 162 (1996)
149. G A Jackson *J. Colloid Interface Sci.* **202** 20 (1998)
150. M Kolb, H J Herrmann *Phys. Rev. Lett.* **59** 454 (1987)
151. T Sintes, R Toral, A Amitabha *Phys. Rev. E* **50** R3330 (1994)
152. M Carpineti, M Giglio *Phys. Rev. Lett.* **68** 3327 (1992)
153. D J Robinson, J C Earnshow *Phys. Rev. Lett.* **71** 715 (1993)
154. M D Haw, W C K Poon, P N Pusey *Physica A* **208** 8 (1994)
155. A Gonzalez, G Ramirez-Santiago *J. Colloid Interface Sci.* **182** 254 (1996)
156. H Furukawa *Adv. Phys.* **34** 703 (1985)
157. H F van Garderen, W H Dokter, T P M Beelen, R A van Santen, E Pantos, M A J Michels, P A J Hilbers *J. Chem. Phys.* **102** 480 (1995)
158. A Hasmy, R Jullien *J. Non-Cryst. Solids* **186** 342 (1995)
159. M Lach-hab, A E Gonzalez, E Blaisten-Barojas *Phys. Rev. E* **54** 5456 (1996)
160. F Sciortino, P Tartaglia *Physica A* **231** 191 (1996)
161. F Sciortino, P Tartaglia *Phys. Rev. Lett.* **74** 282 (1995)
162. M Kolb *J. Phys. A: Math. Gen.* **19** L263 (1986)
163. W Y Shih, J Liu, W H Shih, I A Aksay *J. Stat. Phys.* **62** 1123 (1991)
164. F Family, P Meakin, J M Deutch *Phys. Rev. Lett.*, **57** 727 (1986)
165. I Ya Ladyzhenskii *Kolloid. Zh.* **54** 80 (1992) [b]
166. M D Haw, M Sievwright, W C K Poon, P N Pusey *Adv. Colloid Interface Sci.* **62** 1 (1995)
167. P N Pusey, A D Pirie, W C K Poon *Physica A* **201** 322 (1993)
168. T Hashimoto, M Takenaka, T Izuminati *J. Chem. Phys.* **97** 679 (1992)
169. E Dickinson *J. Chem. Soc., Faraday Trans.* **90** 173 (1994)
170. W C K Poon, M D Haw *Adv. Colloid Interface Sci.* **73** 71 (1997)
171. K Countinho, M A F Gomes, S K Adhikari *Europhys. Lett.* **18** 119 (1992)
172. C Gavrilov, M Sheintuch *Ind. Eng. Chem. Res.* **36** 2915 (1997)
173. F M Gyure, B F Edvards *Phys. Rev. Lett.* **68** 2692 (1992)
174. J M Debierre, R M Bradley *Phys. Rev. E* **53** 1238 (1996)
175. J F Gouyet *Physica A* **168** 581 (1990)
176. J M Debierre *Phys. Rev. Lett.* **78** 3145 (1997)
177. M F Gyure, M V Ferer, B F Edwards, G Huber *Phys. Rev. E* **51** 2632 (1995)
178. H G E Hentschel, I Procaccia *Physica D* **8** 435 (1983)
179. T C Halsey, M H Jensen, L P Kadanoff, I Procaccia, B I Shraiman *Phys. Rev. A* **33** 1141 (1986)
180. P Meakin, J M Deutch *J. Chem. Phys.* **86** 4648 (1987)
181. A Coniglio, L DeArcangelis, H J Herrmann *Physica A* **157** 21 (1989)
182. H E Stanley, P Meakin *Nature (London)* **335** 405 (1988)
183. H E Stanley *Introduction to Phase Transition and Critical Phenomena* (Oxford: Oxford University Press, 1971)
184. M Kohmoto *Phys. Rev. A* **37** 1345 (1988)
185. M A Lopez-Quintela, M C Bujan-Nunez *Mol. Phys.* **77** 857 (1992)
186. M A Lopez-Quintela, C Tojo M C Bujan-Nunez *Mol. Phys.* **74** 785 (1991)
187. A Bershadskii *Physica A* **253** 23 (1998)
188. M Walf *J. Phys. A: Math. Gen.* **23** L1287 (1990)
189. A Block, W von Bloch, H J Schellnhuber *Phys. Rev. A* **42** 1869 (1990)
190. W G Hanan, D M Heffernan, J C Earnshaw *Chaos, Solitons Fractals* **9** 875 (1998)
191. M E Cates, J M Deutch *Phys. Rev. A* **35** 4907 (1987)
192. P Pastor-Satorras, J Wagensberg *Physica A* **224** 463 (1996)
193. P Pastor-Satorras, J Wagensberg *Physica A* **251** 291 (1998)
194. F Martinez-Lopez, M A Cabrerizo-Vilchez, R Hidalgo-Alvarez *Physica A* **291** 1 (2001)
195. J H J van Opheusden *Physica A* **252** 10 (1998)
196. B Dubuc, J-C Quiniou, C Roques-Carmes, C Tricot, S W Zucker *Phys. Rev. A* **39** 1500 (1989)
197. D Hamburger, O Biham, D Avnir *Phys. Rev. E* **53** 3342 (1996)
198. P Hildgen, F Nekka, F Hildgen, J N McMullen *Physica A* **234** 593 (1997)
199. S Buczkowski, P Hildgen, L Cartilier *Physica A* **252** 23 (1998)
200. M Thorn, M Seesselberg *Phys. Rev. Lett.* **72** 3622 (1994)
201. M Kolb, H J Herrmann *J. Phys. A: Math. Gen.* **18** L435 (1985)
202. A Hasmy, E Anglaret, M Foret, J Pelous, R Jullien *Phys. Rev. B* **50** 6006 (1994)
203. E Dickinson *J. Chem. Soc., Faraday Trans.* **93** 111 (1997)
204. M Hutter *J. Colloid Interface Sci.* **231** 337 (2000)
205. B H Bijsterbosch, M T A Bos, E Dickinson, J H J van Opheusden, P Walstra *Faraday Discuss.* **101** 51 (1995)
206. J F M Lodge, D M Heyes *J. Chem. Soc., Faraday Trans.* **93** 437 (1997)
207. K G Soga, J R Melrose, R C Ball *J. Chem. Phys.* **108** 6026 (1998)
208. R Yamahara, K Okazaki *Fluid Phase Equilib.* **144** 449 (1998)
209. L J B Bremer, B H Bijsterbosch, P Walstra, T van Vliet *Adv. Colloid Interface Sci.* **46** 117 (1993)
210. J C Pouxviel, J P Boilot, A Dauger, A Wright *J. Non-Cryst. Solids* **103** 331 (1988)

211. E K Hobbie, B J Bauer, C C Han *Phys. Rev. Lett.* **72** 1830 (1994)
212. J Bibette, T G Mason, H Gang, D A Weitz *Phys. Rev. Lett.* **69** 981 (1992)
213. J Bibette, T G Mason, H Gang, D A Weitz, P Poulin *Langmuir* **9** 3352 (1993)
214. W C K Poon, A D Pirie, P N Pusey *Faraday Discuss.* **101** 65 (1995)
215. A Hamsy, M Foret, E Anglaret, J Pelous, R Vacher, R Jullien *J. Non-Cryst. Solids* **186** 118 (1995)
216. M D Haw, M Sievwright, W C K Poon, P N Pusey *Physica A* **217** 231 (1995)
217. M Kolb *Polym. Gels Netw.* **4** 375 (1996)
218. R Rodriguez, G Rojas, M Estevez, S Vargas *J. Sol-Gel Sci. Technol.* **23** 99 (2001)
219. D W Schaefer, T Rieker, M Agamalian, J S Lin, D Fischer, S Sukumaran, C Chen, G Beaucage, C Herd, J Ivie *J. Appl. Crystallogr.* **33** 587 (2000)
220. T P M Beelen, W Shi, G R Morrison, H F van Garderen, M T Browne, R A van Santen, E Pantos *J. Colloid Interface Sci.* **185** 217 (1997)
221. Y Liu, R B Pandey *Phys. Rev. B* **55** 8257 (1997)
222. E Dickinson *J. Colloid Interface Sci.* **225** 2 (2000)
223. J F M Lodge, D M Heyes *Phys. Chem. Chem. Phys.* **1** 2119 (1999)
224. M T A Bos, J H J van Opheusden *Phys. Rev. E* **53** 5044 (1996)
225. J F M Lodge, D M Heyes *J. Chem. Phys.* **109** 7567 (1998)
226. B Knoblich, Th Gerber *J. Non-Cryst. Solids* **283** 109 (2001)
227. F Gaboriaud, D Chaumont, A Nonat, A Craievich *J. Appl. Crystallogr.* **33** 597 (2000)
228. M Mellema, J H vanOpheusden, T vanVliet *J. Chem. Phys.* **111** 6129 (1999)
229. L R B Santos, A F Craievich, C V Santilli, S H Pulcinelli *J. Appl. Crystallogr.* **33** 609 (2000)
230. J A Chaker, K Dahmouche, A F Craievich, C V Santilli, S H Pulcinelli *J. Appl. Crystallogr.* **33** 700 (2000)
231. L Matejka, J Pestil, K Dusek *J. Non-Cryst. Solids* **226** 114 (1998)
232. P R Williams, R L Williams, R Jones, A Al-Hussany, S Ravji *J. Non-Cryst. Solids* **293–295** 731 (2001)
233. S D Romano, D H Kurlat *Chem. Phys. Lett.* **323** 93 (2000)
234. F Bordi, C Cametti, P Codastefano, P Tartaglia *Physica A* **164** 663 (1990)
235. L Cipelletti, S Manley, R C Ball, D A Weitz *Phys. Rev. Lett.* **84** 2275 (2000)
236. A H Krall, D A Weitz *Phys. Rev. Lett.* **80** 778 (1998)
237. S Guillot, D Lairez, M A V Axelos *J. Appl. Crystallogr.* **33** 669 (2000)
238. A A Lushnikov, A E Negin, A V Pakhomov *Chem. Phys. Lett.* **175** 138 (1990)
239. B Schleicher, S K Friedlander *J. Colloid Interface Sci.* **180** 15 (1996)
240. C M Sorensen, W B Hageman, T J Rush, H Huang, C Oh *Phys. Rev. Lett.* **80** 1782 (1998)
241. R Brunner, S Gall, W Wilke, M Zrinyi *Physica A* **239** 477 (1997)
242. P Argyrakis, G Duportail, P Lianos *J. Chem. Phys.* **95** 3808 (1991);
243. G Duportail, J-C Brochon, P Lianos *J. Phys. Chem.* **96** 1460 (1992)
244. M I Ozhovan *Zh. Ekp. Teor. Fiz.* **104** 4021 (1993) [g]
245. V V Zosimov, D N Tarasov *Zh. Eksp. Teor. Fiz.* **111** 1314 (1997) [g]
246. M Lagues, C Sauterey *J. Phys. Chem.* **84** 3503 (1980)
247. S Skaf, G Stell *Phys. Rev. A* **46** R3020 (1992)
248. S H Chen, J Rouch, F Sciortino, P Tartaglia *J. Phys.: Condens. Matter* **6** 10 855 (1994)
249. C M McCallum, J R Gun *Phys. Rev. E* **55** 1201 (1997)
250. S A Safran, I Webman *Phys. Rev. A* **32** 506 (1985)
251. P Tartaglia, J Rouch, S H Chen *Phys. Rev. A* **45** 7257 (1992)
252. F Mallamace, N Micali *Croat. Chem. Acta* **65** 379 (1992)
253. M Mays *J. Phys. Chem. B* **101** 10271 (1997)
254. B Antalek, A J Williams, J Texter *Phys. Rev. E* **54** R5913 (1996)
255. C M C Gambi, M G Giri, M Carla, D Senatra A Chittofrati *Phys. Rev. E* **56** 4356 (1997)
256. E Michel, M Filani, R Aznar, G Porte, J Appell *Langmuir* **16** 8702 (2000)
257. A I Fisenko, S Magazu, G Maisano, N P Malomuzh *Nuovo Cimento Soc. Ital. Fis., D* **20** 675 (1998)
258. K Kawasaki, T Kawakatsu *Physica A* **164** 549 (1990)
259. T Kawakatsu, K Kawasaki *Physica A* **167** 690 (1990)
260. T Kawakatsu, K Kawasaki, M Furusaka, H Okabayashi, T Kanaya *J. Phys.: Condens. Matter* **6** 6385 (1994)
261. D Chowdhury *J. Phys.: Condens. Matter* **6** 2435 (1994)
262. P Pieruschka, S A Safran *J. Phys.: Condens. Matter* **6** A357 (1994)
263. A Hurd, D W Schaefer *Phys. Rev. Lett.* **54** 1043 (1985)
264. G Y Onada *Phys. Rev. Lett.* **55** 226 (1985)
265. D J Robinson, J C Earnshow *Phys. Rev. A* **46** 2045 (1992)
266. D J Robinson, J C Earnshow *Phys. Rev. A* **46** 2055 (1992)
267. D J Robinson, J C Earnshow *Phys. Rev. A* **46** 2065 (1992)
268. Z Horvölgyi, G Medveczky, M Zrinyi *Colloids Surf.* **60** 79 (1991)
269. Z Horvölgyi, G Medveczky, M Zrinyi *Colloid Polym. Sci.* **271** 396 (1993)
270. Z Horvölgyi, M Mate, M Zrinyi *Colloids Surf. A* **84** 207 (1994)
271. J Ruiz-Garcia, B Ivlev *Mol. Phys.* **95** 371 (1998)
272. A Vincze, R Fata, M Zrinyi, Z Horvolgyi, J Kertesz *J. Chem. Phys.* **107** 7451 (1997)
273. L Zeiri, S Efrima, M Deutsch *J. Phys. Chem. B* **101** 9757 (1997)
274. D Yogev, S Efrima *J. Phys. Chem.* **92** 5754 (1988)
275. J C Earnshaw, D J Robinson *J. Phys.: Condens. Matter* **7** L397 (1995)
276. J C Earnshaw, M B Harrison, D J Robinson *Phys. Rev. E* **53** 6155 (1996)
277. P H F Hansen, L Bergström *J. Colloid Interface Sci.* **218** 77 (1999)
278. A Gonzales, F Martinez-Lopez, A Moncho-Jorda, R Hidalgo-Alvarez *J. Colloid Interface Sci.* **246** 227 (2002)
279. D B Berg *Pis'ma ZhTF* **25** (23) 81 (1999) [d]
280. F Chezzi, J C Earnshaw, M Finnis, M VcCluney *J. Colloid Interface Sci.* **238** 433 (2001)
281. Y Jin, S Dong *Angew. Chem., Int. Ed.* **41** 1040 (2002)
282. D Kessler, H Levine *Phys. Rev. Lett.* **67** 3121 (1991)
283. G Fucks, P Melinon, F Santos Aires, M Treilleux, B Cabaud, A Hoareau *Phys. Rev. B* **44** 3926 (1991)
284. A Perez, P Melion, V Dupuis, P Jensen, B Prevel, J Tuaillon, L Bardotti, C Martet, M Treilleux, M Broyer, M Pellarin, J L Vaille, B Palpant, J Lerme *J. Phys. D: Appl. Phys.* **30** 709 (1997)
285. P Jensen *Rev. Mod. Phys.* **71** 1695 (1999)
286. T C Chang, I S Hwang, T T Tsong *Phys. Rev. Lett.* **83** 1191 (1999)
287. V D Borman, A V Zenkevich, M A Pushkin, V N Tronin, V I Troyan *Pis'ma ZhETF* **73** 684 (2001) [c]
288. V D Borman, A V Zenkevich, S Ch Lai, V N Nevolin, M A Pushkin, V N Tronin, V I Troyan, Dzh Sheval'e *Pis'ma ZhETF* **72** 216 (2000) [c]
289. Z Zhang, X Chen, M G Lagally *Phys. Rev. Lett.* **73** 1829 (1994)
290. M B Luo, G X Ye, A G Xia, J S Jin, B Yang, J M Xu *Phys. Rev. B* **59** 3218 (1999)
291. P Jensen, A Barabasi, H Larralde, S Havlin, H E Stanley *Phys. Rev. B* **50** 15316 (1994)
292. N V Brilliantov, Yu A Andrienko, P L Krapivsky, J Kurths *Phys. Rev. Lett.* **76** 4058 (1996)
293. M K Hassan *Phys. Rev. E* **55** 5302 (1997)
294. D A Lidar (Hamburger), O Biham, D Avnir *J. Chem. Phys.* **106** 10359 (1997)
295. R Q Hwang, J Schroder, C Gunther, R J Behm *Phys. Rev. Lett.* **67** 3279 (1991)
296. T Michely, M Hohage, M Bott, G Cosma *Phys. Rev. Lett.* **70** 3943 (1993)
297. G X Ye, Th Michely, V Weidenhof, I Friedrich, M Wuttig *Phys. Rev. Lett.* **81** 622 (1998)
298. K Soleka-Cermakova, B Vickova, F Lednicky *J. Phys. Chem.* **100** 4954 (1996)
299. S Matsushita, T Miwa, A Fujishima *Langmuir* **13** 2582 (1997)
300. V G Myagkov, L I Kveglis, V S Zhigalov *Poverkhnost'* (6) 46 (1995)
301. J M Chabalda *Phys. Rev. B* **46** 11346 (1992)

302. V G Myagkov, V S Zhigalov, S M Zharkov *Dokl. Akad. Nauk* **346** 612 (1996) [h]
303. V I Zyn', S L Molchatskii *Poverkhnost* (4) 66 (1999)
304. D V Novikov, A N Krasovskii, A Andreeva, S V Basov *Kolloid. Zh.* **61** 240 (1999) [b]
305. J S Langer *Rev. Mod. Phys.* **52** 1 (1980)
306. D A Kessler, J Koplik, H Levine *Adv. Phys.* **37** 255 (1988)
307. G M Homsy, in *Disorder and Mixing* (Ed. E Guyon) (Dordrecht: Kluwer Academic, 1988) p. 237
308. G M Homsy *Annu. Rev. Fluid Mech.* **19** 271 (1987)
309. D Bensimon *Phys. Rev. A* **33** 1302 (1986)
310. S S S Cardoso, A W Woods *J. Fluid Mech.* **289** 351 (1995)
311. H Tang, W Grivas, D Homentcovschi, J Geer, T Singler *Phys. Rev. Lett.* **85** 2112 (2000)
312. L Paterson *Phys. Rev. Lett.* **52** 1621 (1984)
313. A J DeGregoria *Phys. Fluids* **28** 2933 (1985)
314. M Sahimi, H Siddiqui *J. Phys. A: Math. Gen.* **20** L89 (1987)
315. C-T Tan, G M Homsy *Phys. Fluids A: Fluid. Dyn.* **4** 1099 (1992)
316. Y Meir, A Aharony *Physica A.* **157** 524 (1989)
317. P Meakin *Physica A* **173** 305 (1991)
318. G Wagner, P Meakin, J Feder, T Jshssang *Phys. Rev. E* **55** 1698 (1997)
319. K E Tompson, H S Fogler *Phys. Rev. E* **57** 5825 (1998)
320. W B Zimmerman, G M Homsy *Phys. Fluids A: Fluid. Dyn.* **4** 1901 (1992)
321. J Krug, P Meakin *Phys. Rev. Lett.* **66** 703 (1991)
322. G Daccord *Phys. Rev. Lett.* **58** 479 (1987)
323. G Daccord, R Lenormand *Nature (London)* **325** 41 (1987)
324. T Nagatani, J Lee, H E Stanley *Phys. Rev. Lett.* **66** 616 (1991)
325. C D Tsakiroglou, A C Payatakes *Adv. Colloid Interface Sci.* **75** 215 (1998)
326. D Wilkinson, J F Willemsen *J. Phys. A* **16** 3365 (1983)
327. R Lennormand, E Toubol, C Zarcone *J. Fluid Mech.* **189** 165 (1988)
328. M Cieplak, A Maritan, J R Banavar *Phys. Rev. Lett.* **76** 3754 (1997)
329. M Porto, S Havlin, S Schwarzer, A Bunde *Phys. Rev. Lett.* **79** 4060 (1997)
330. M Sahimi, M Hashemi, J Ghassemzadeh *Physica A* **260** 231 (1998)
331. D W Zheng, W Wen, K N Tu *Phys. Rev. E* **57** R3719 (1998)
332. V Traskine, P Protsenko, Z Skvortsova, P Volovitch *Colloids Surf. A* **166** 261 (2000)
333. J Lapujoule *Surf. Sci. Rep.* **20** 191 (1994)
334. F Family, T Visceck (Eds) *Dynamics of Fractal Surfaces* (Singapore: World Scientific, 1991)
335. F Family, T Vicsek *J. Phys. A: Math. Gen.* **18** L1163 (1985)
336. R Jullien, R Botet *Phys. Rev. Lett.* **54** 2055 (1985)
337. P Meakin *J. Phys. A: Math. Gen.* **20** L1113 (1987)
338. S F Edwards, D R Wilkinson *Proc. R. Soc. London, Ser. A* **381** 17 (1982)
339. D A Kessler, H Levine, Y Tu *Phys. Rev. A* **43** 4551 (1991)
340. G Zumofen, J Klafter, A Blumen *Phys. Rev. A* **45** 8977 (1992)
341. G Poupart, G Zumofen *Phys. Rev. E* **50** R663 (1994)
342. R C Salvarezza, L Vazquez, H Miguez, R Mayorala, C Lopez, F Meseguer *Phys. Rev. Lett.* **77** 4572 (1996)
343. X-Y Lei, P Wan, C-H Zhou, N-B Ming *Phys. Rev. E* **54** 5298 (1996)
344. M Kardar, G Parisi, Y-C Zhang *Phys. Rev. Lett.* **56** 889 (1986)
345. J Krug *Phys. Rev. A* **36** 5465 (1987)
346. J G Amar, F Family *Phys. Rev. A* **45** R3373 (1992)
347. J G Amar, F Family *Phys. Rev. A* **45** 5378 (1992)
348. Z W Lai, S Das Sarma *Phys. Rev. Lett.* **66** 2348 (1991)
349. A L Barabasi, H E Stanley *Fractal Concepts in Surface Growth* (Cambridge: Cambridge University Press, 1995)
350. L Golubovich, R Bruinsma *Phys. Rev. Lett.* **66** 321 (1991)
351. I Procaccia, M H Jensen, V S L'vov, K Sneppen, R Zeitak *Phys. Rev. A* **46** 3220 (1992)
352. A L Barabasi *Phys. Rev. A* **46** R2977 (1992)
353. Y Tu *Phys. Rev. A* **46** R729 (1992)
354. F Leonard, R C Desai *Phys. Rev. B* **55** 9990 (1997)
355. O Gat, Z Olami *Phys. Rev. E* **56** 1714 (1997)
356. M T Batchelor, B I Henry, S D Watt *Physica A* **260** 11 (1998)
357. H F Nashar, W Wang, H A Cerdeira *Surf. Sci.* **391** 1 (1997)
358. J O Indekeu, G Fleerackers *Physica A* **261** 294 (1998)
359. R Chiarello, V Panella, J Krim, C Thompson *Phys. Rev. Lett.* **67** 3408 (1991)
360. P Herrasti, P Ocon, L Vazquez, R C Salvarezza, J M Vara, A J Ariva *Phys. Rev. A* **45** 7440 (1992)
361. R C Salvarezza, L Vazquez, P Herasti, P Ocon, J M Vara, A J Ariva *Europhys. Lett.* **20** 727 (1992)
362. Z H Liu, N M D Brown, A MaKinley *J. Phys.: Condens. Matter* **9** 59 (1997)
363. C Tompson, C Palasantzaz, Y P Feng, S K Sinha, J Krim *Phys. Rev. B* **49** 4902 (1994)
364. J Krim, I Heyvaert, C van Haesendock, Y Bruynseraede *Phys. Rev. Lett.* **70** 57 (1993)
365. Y-L He, H-N Yang, T-M Lu, G-C Wang *Phys. Rev. Lett.* **69** 3770 (1992)
366. H-N Yang, T-M Lu, G-C Wang *Phys. Rev. B* **47** 3911 (1993)
367. A I Oliva, E Anguiano, J L Sacedon, M Aguilar, J A Mendez, J A Aznarez *Phys. Rev. B* **60** 2720 (1999)
368. S V Buldyrev, A-L Barabashi, F Castera, S Havlin, H E Stanley, T Vicsek *Phys. Rev. A* **45** R8313 (1992)
369. V K Horvath, H E Stanley *Phys. Rev. E* **52** 5166 (1995)
370. T H Kwon, A E Hopkins, S E O'Donnell *Phys. Rev. E* **54** 685 (1996)
371. J Zhang, Y-C Zhang, P Alstrom, M T Levinsen *Physica A* **189** 383 (1992)
372. J Kertesz, V K Horvath, F Weber *Fractals* **1** 67 (1993)
373. H Yan *Phys. Rev. Lett.* **68** 3048 (1992)
374. S Miyazima, H Yoshinaga, T Nagamine, H Takano, J Kertesz, H E Stanley *Physica A* **259** 1 (1998)
375. G S Frankel *Corros. Sci.* **30** 1203 (1990)
376. J M Costa, F Sagues, M Vilarrasa *Corros. Sci.* **32** 665 (1991)
377. L Balazs, L Nyikos, I Sabo, R Schiller *Fractals* **1** 319 (1993)
378. L Balazs *Phys. Rev. E* **54** 1183 (1996)
379. T Johnsen, A Jøssang, T Jøssang, P Meakin *Physica A* **242** 356 (1997)
380. A Hernandez Creus, P Carro, R C Salvarezza, A J Arvia *Langmuir* **13** 833 (1997)

[a] — *Physics-Uspekhi (Engl. Transl.)*
[b] — *Colloid. J. (Engl. Transl.)*
[c] — *J. Exp. Theor. Phys. Lett. (Engl. Transl.)*
[d] — *Techn. Phys. Lett. (Engl. Transl.)*
[e] — *Crystallogr. Rep. (Engl. Transl.)*
[f] — *Polym. Sci. (Engl. Transl.)*
[g] — *J. Exp. Theor. Phys. (Engl. Transl.)*
[h] — *Dokl. Phys. (Engl. Transl.)*